Active tectonics of the Ganzi-Yushu fault in the southeastern Tibetan Plateau

Feng Shi[1], Honglin He[1], Alexander L. Densmore[2], An Li[3], Xiaoping Yang[1], Xiwei Xu[1]

1 Key Laboratory of Active Tectonics and Volcano, Institute of Geology, China Earthquake Administration, Beijing 100029, China.

2 Institute of Hazard and Risk Research and Department of Geography, Durham University, Durham, UK.

3 Key Laboratory of Crustal Dynamics, Institute of Crustal Dynamics, China Earthquake Administration, Beijing 100085, China.

Abstract: The ongoing convergence between India and Eurasia apparently is accommodated not merely by crustal shortening in Tibet, instead also by motions along strike slip faults which are usually boundaries between tectonic blocks, especially in the Tibetan plateau. Quantification of this strike slip faulting is fundamental for understanding the collision between India and Eurasia. Here, we use a variety of geomorphic observations to place constraints on the late Quaternary kinematics and slip rates of the Ganzi-Yushu fault, one of the significant strike-slip faults in eastern Tibet. The Ganzi-Yushu fault is an active, dominantly left-lateral strike-slip structure that can be traced continuously for up to 500 km along the northern boundary of the clockwise-rotating southeastern block of the Tibetan Plateau. We analyse geomorphic evidence for deformation, and calculate the late Quaternary slip rates at four sites along the eastern portion of the fault trace. Latest Quaternary apparent throw rates are variable along strike but are typically ~1 mm/a. Rates of strike-slip displacement are likely to be an order of magnitude higher, 8-11 mm/a. Trenching at two locations suggest that the active fault behaviour is dominated by strike-slip faulting and reveal

several earthquake events with refined information of timing. . The 2010 M_w6.9 Yushu earthquake, which occurred on the northwestern segment of the Ganzi-Yushu fault zone, provides additional evidence for fault activity. These observations agree with GPS-derived estimates, and show that late Quaternary slip rates on the Ganzi-Yushu fault are comparable to those on other major active strike-slip faults in the eastern Tibetan Plateau.

Keywords: Ganzi-Yushu fault, late Quaternary, active faulting, slip rates, India-Asia collision

1. Introduction

The ongoing convergence between India and Eurasia apparently is accommodated not merely by crustal shortening in Tibet, instead also by motions along strike slip faults which are usually boundaries between tectonic blocks, especially in the Tibetan plateau [Molnar and Tapponnier, 1978]. To explain this deformation, two influential end-member views of continental deformation have been debated during the last several decades: (1) block models, in which intracontinental deformation can be concentrated on major faults separating a number of relatively rigid blocks[e.g., Dewey et al., 1973; Avouac and Tapponnier, 1993; Peltzer and Saucier, 1996; Tapponnier et al., 2001; Meade, 2007; Thatcher, 2007]; or (2) continuum models, in which deformation is regionally distributed in the shallow brittle crust, and is essentially continuous at depth[e.g., Molnar and Tapponnier,1975; England and McKenzie, 1982; England and Houseman, 1986;]. When the two views are applied to eastern Asia, large slip rates on major faults are required by block models, but not by continuum models. Thus, documentation and quantification

of kinematics and slip rates on the major strike slip faults, along with observations of historical earthquake activity, are fundamental for understanding the collision between India and Eurasia.

The four major earthquakes (M_w>7.0) which occurred in the Tibetan Plateau during the last two decades (1997 M_w7.5 Manni earthquake [Xu, 2000], 2001 M_w7.8 Kunlunshan earthquake [Xu et al., 2002], 2008 M_w7.2 Yutian earthquake [Xu et al., 2011] and 2008 M_w7.9 Wenchuan earthquake [Xu et al., 2009]), and the 2010 M_w6.9 Yushu earthquake, all occurred around the boundaries of the Bayan Har fault-block (Figure 1), also known as the Songpan block [Thatcher, 2007] or Kunlun block [Gan et al., 2007], sourrounding by Longmenshan Fault (east boundary), Xianshuihe Faunt and Ganzi-Yushu fault (south boundary), Kunlun fault (north boundary). The published GPS velocities [e.g. Wang et al., 2001; Gan et al., 2007; Thatcher, 2007] suggest the southward movement of the Bayan Har fault-block relative to stable Eurasia, but the mechanisms and starting time of this movement have been a matter of debate [Chen et al., 1994; Kirby et al., 2000, 2002, 2003; Clark et al., 2005]. The eastern boundary faults of the block accommodated significant crustal shortening during the Late Triassic Indosinian Orogeny [Chen and Wilson, 1996; Li et al., 2003], and the Longmen Shan region at the eastern margin of the block has been identified as a major thrust zone that was reactivated in the India-Asia collision [e.g., Avouac and Tapponnier, 1993; Xu and Kamp, 2000].The northern and southern boundaries of the block are major left-lateral strike-slip faults – the Ganzi-Yushu and Xianshuihe fault system to the south, and the Kunlun fault system to the north.

In order to understand the mechanism of the Bayan Har fault-block in the India-Asia collision, the

66 late Cenozoic activity and kinematics of the major faults along the block margins must be
67 documented. Much work about the late Cenozoic activity and kinematics of faults in the Longmen
68 Shan has been done by Chen et al. [1994], Burchfiel et al. [1995] and Densmore et al. [2007].The
69 slip rates of the Xianshuihe and Kunlun faults have been well constrained [e.g. Allen et al., 1991;
70 Van der Woerd et al., 2002], there are also many results of slip rate on Ganzi-Yushu fault from
71 fieldwork [Zhou et al., 1996; Wen et al. 2003; Peng et al., 2006] and GPS[Wang et al., 2001; Shen
72 et al., 2005; Gan et al., 2007; Wang, 2009]. Tapponnier et al. [2001] and others inferred fast rates,
73 about 15 mm/a, to argue for rigid-block extrusion, but others [e.g., England and Molnar, 2005]
74 have suggested that slow rates, about 5 mm/a or slower, are consistent with continuous
75 deformation. The kinematics of the Ganzi-Yushu fault, its slip rate, and the timing of
76 paleoearthquakes on the fault all remain poorly constrained. Some slip rates have been obtained
77 from terrace or alluvial fan offsets along with age estimates from TL (thermoluminescence) dating
78 [Zhou et al., 1996; Wen et al. 2003]. There has also been some work using river offsets, although
79 the ages of these offsets were only loosely constrained as Holocene [Peng et al., 2006]. The huge
80 range of the slip rates, which from 3 mm/a to 13 mm/a, couldn't test different deformation models.
81 The reasons of the huge range come from two aspect, one is the dating method and another is the
82 choice of offset markers. Moreover, because of the high altitude and remoteness of the fault,
83 there has been very little work on paleoearthquakes in these areas.
84
85 We address the fault trace by presenting geomorphic evidence for deformation along the
86 Ganzi-Yushu fault, and constrain the fault behaviour by paleoseismology. We use a combination of
87 techniques, including field mapping, image interpretation, surveying of offset geomorphic markers,

and trenching, in order to examine the history of fault slip over the last few thousand years.

2 Geological setting

The Ganzi-Yushu fault zone forms part of the boundary between the Qiangtang and Bayan Har blocks in the eastern Tibetan Plateau [Zhang et al., 2003; He et al., 2006]. The Ganzi-Yushu fault zone can be traced for ~500 km along strike and consists of a series of generally NW-striking fault segments. The western most tip of the fault zone occurs near Qutang township, in Zhiduo county of Qinghai Province, and the fault extends eastward through Dangjiang, Yushu, Dengke, and Yulong townships to end at Ganzi county in Sichuan Province. Where it is visible at the surface, the fault appears to dip 70-85°NE near the surface, except for a SW-dipping segment near Tuodang township [Li et al., 1995]. The 2010 M_w 6.9 Yushu earthquake ruptured the Ganzi-Yushu fault over a total distance of about 50 km [Chen et al. 2010; Li et al., 2012]. Focal mechanism solutions [Chen, 2010; USGS, 2010] and displaced geomorphic features indicate that the earthquake rupture is nearly pure left-lateral strike-slip with a minor SW dip-slip component.

Exposures of the active Ganzi-Yushu fault show that it coincides with zones of dense fracturing in pre-Quaternary bedrock; the widths of these zones is generally ~10-50 m but is rarely up to a few hundred meters [Zhou et al., 1996]. In remote sensing imagery, strands of the fault form clear linear features associated with scarps, shutter ridges, and offset drainages characteristic of active strike-slip deformation [Zhou et al., 1996]. The fault movement appears to be dominated by left-lateral strike-slip, with little consistent net vertical slip [Peng et al., 2006].

Previously-published estimates of strike-slip rates span a large range from 3 mm/a to 14 mm/a (Figure 2) [Zhou et al., 1996; Wen et al., 2003; Peng et al., 2006]. Many of these are based on

low-resolution geomorphic markers (e.g., river offsets) and on imprecise or relative dating techniques. Based on GPS velocities, the Ganzi-Yushu fault has an estimated strike-slip rate of 10 mm/a to 16 mm/a, depending on the tectonic model that is used (Figure 2) [Wang et al., 2001; Shen et al., 2005; Gan et al., 2007; Wang, 2009].

3 Methods and techniques

3.1 Fault mapping

We focus our attention on the southeastern 150 km of the Ganzi-Yushu fault zone. This is because (1) the northwestern strands of the fault are relatively inaccessible, and (2) Quaternary deposits that could be used to indicate the kinematics and timing of recent deformation are more extensively exposed along the southeastern portion of the fault zone (Figure 1). We mapped the active traces of the southeastern Ganzi-Yushu fault zone with CBERS (China-Brazil Earth Resources Satellite) imagery (2.36 m spatial resolution) and Chinese aerial photographs (~1 m spatial resolution). We then made field observations at sites with geomorphic indicators of late Quaternary activity, including scarps or offset surfaces in Quaternary deposits, offset channels, shutter ridges and linear valleys. Offset landforms were surveyed using a differential GPS (DGPS) measuring system, with a measurement repeatability of better than ±10 cm. If the offsets were too large to be measured by field surveys, we estimated the offsets from the CBERS imagery and aerial photographs.

Much of the evidence for active faulting comes from offset or truncated fluvial fill terraces. We mapped these terraces on aerial photographs, supplemented with field investigations. Fill terraces in this region are typically composed of subhorizontal, crudely- to well-bedded gravel and sand layers. We identified terrace surfaces, and assigned relative ages, on the basis of relative height between the surface and the modern river bed. At each site, terraces were numbered in ascending order from youngest (T0, representing the modern floodplain) to oldest. We determined absolute ages of fill terrace deposition and abandonment using ^{14}C dating of samples in sand layers. We lack sufficient data to assess whether terrace ages can be correlated between different sites along the Ganzi-Yushu fault, or whether the terrace chronology is site-specific.

Although the strike-slip component is dominant along the entire fault, the ratios of strike-slip and vertical offsets, and the strike-slip rates, are not uniform along strike. With this in mind, we describe our observations below in terms of strike-slip and vertical offsets. Throw rates are regarded as consistent along each fault segment, but the ratio and the strike-slip rates have a tendency to decline from west to east, toward the fault tip.

3.2 Trenching

To establish the timing of the most recent slip on the fault, we excavated several trenches across the Ganzi-Yushu fault at two separate sites. Accurate fault traces and sufficient sediment accumulation with organic material are fundamental for trenching. In Renguo township (Figure 2), we excavated a 2-m-deep trench across the fault. This site is located at a well-developed fault

scarp on a terrace surface near the estimated epicenter of the 1854 earthquake [Wen et al., 2003]. The steep terrain south of the site has trapped sediment, providing sufficient organic material. Because a distinctive layer was found in the west wall of the trench, but not in the east wall, we excavated a second 2-m-deep trench at right angles to the first, parallel to the fault, in order to reconstruct a horizontal piercing line. To assess possible differences in fault activity between different segments, we excavated a 3-m-deep trench across the fault at Cuoa township (Figure 2).This site is also located on a terrace surface. The fault plane is exposed in the terrace riser, allowing accurate determination of the fault position, and the steep terrain to the south of the site provides sufficient sediment accumulation and organic material. All trench walls were cleaned and logged at a scale of 1:10 following standard procedures [e.g., McCalpin, 1996]. Depositional ages of the units in the trench faces were provided by ^{14}C analysis of charcoal fragments from Beta Analytic Radiocarbon Dating Laboratory.

4 Results

We can trace the southeastern Ganzi-Yushu fault continuously for approximately 150 km. The fault shows clear evidence for Quaternary sinistral strike-slip displacement, with minor components of dip slip.

4.1 Shengkang

Shengkang (Figure 2) was severely damaged by the 1854 earthquake [Wen et al., 2003]. On aerial photographs, there are obvious offsets of fill terraces at this site (Figure 3). The fault has caused sinistral strike-slip displacement of the T5/T3 riser by approximately 350 m, and a vertical offset

of the T5 surface by ~50 m (Figure 3).The ages of T5 and T3 at this site have been estimated at 46100±3500 a and 16290±1200 a based on TL dating [Wen et al., 2003]. But Wen et al. [2003] estimate the sinistral-slip rate as 11.5±2.4 mm/a using the mean date between ages of T5 and T3, and inistral strike-slip displacement of the T5/T3 riser, and not estimate the throw rate. The age of T5 is older twice than the age of T3, and the difference between the ages of T5 and T3 is nearly 30000 a. Base on geomorphologic analysis, we hold the opinion that estimating the sinistral-slip rate of 8±1 mm/a and the throw rate of 1±0.1mm/a using the age of T5 is more suitable. No other clear terrace offsets are preserved at this site.

4.2 Renguo

Near Renguo township, a fault scarp let probably associated with the 1854 earthquake, trending 300°with a height of 0.5-1.5m, can be traced for 3 km across on a gently sloping piedmont (Figure 4a, b, c). The fault scarp extends southeast to Ezhong village and dislocates a footpath (Figure 4f), which was built in an ephemeral gully. The eastern boundary of the path shows a sinistral offset of 3m, as does the gully axis. The fault scarp extends northwest to Kagong township and produces a 200m long sag-pond (Figure 4d). According to the leader of Renguo village, there was a village in this region in the past, which was abandoned about 100 years ago. This event may be related to the occurrence of the earthquake in 1854, with an epicenter located near Renguo township [Wen et al., 2003].

191 The trench at Renguo township was excavated across the fault scarp (Figure 3).Six distinct
192 lithologic units were identified in the trench walls, and are described in detail in Table 1. Four
193 fault planes have been recognized in the trench:Fault F1 cuts the lower units and terminates in
194 U1-1. No wedge or flower structure are found at the upper termination of the fault plane. Faults F2
195 cuts unit U1-1, and is overlain by scarp-fill wedges A and B. Scarp-fill edge A is dislocated by F2
196 in the east wall of RGTC1, while some gravel is aligned along the fault in the west wall of RGTC1
197 (Figure 4a). Fault F3 cuts unit U1-1, and appears to terminate at the base of U2. The fault is
198 expressed as a disturbed zone 10-15 cm wide, and creates an uneven base of U2. Fault F4 cuts
199 units U1-1, U2, and U3, and appears to terminate at the base of U4-1. On the east wall of the
200 trench, the fault is associated with an irregularly-shaped deposit of massive or structure less fine
201 gravel.
202
203 Examination of both the fault-normal and fault-parallel trench walls shows that unit U3 pinches
204 out to the east on both the northeast and southwest sides of the fault (Figure 5e). We use the
205 pinch-out position as a piercing line, and estimate that it has been offset by 7.5 ± 0.5 m of sinistral
206 strike-slip and 1 ± 0.2 m of vertical displacement, with the southern or hanging wall block
207 upthrown.
208
209 We infer that two paleoearthquake events are recorded in the Renguo trenches. The first
210 paleoearthquake event occurred after U1 was deposited. Faults F2 and F3 were activated and
211 wedge A was deposited over F2 in this event. The overlying layer U2 is disturbed and has an
212 undulating base over fault F3. We interpret that U2 was being actively deposited when the first

paleoearthquake event occurred and continued to deposit after the earthquake. For this reason, U2 is only deformed near its base, and becomes more flat-lying further up-section. A ^{14}C sample from the base of U2 yields an age of 3030-2885 BC. This is a maximum age for the first paleoearthquake event. The second event occurred after U3 had been deposited, and is marked by dislocation of unit U3 by F4 on the west wall of the trench. This may have been accompanied by remobilization of U3 gravel as a massive deposit along F4. F4 is not clear on the east wall, and no evident deformation was seen in unitU3, which does not appear in the footwall. The gravel deposit along F4 yields a ^{14}C age of 905-795 BC, while a sample from U3 yields an age of 770-475 BC. We use OxCal 4.2.4 (Bronk Ramsey, 2013) by 6 ^{14}C age (RGTC1-W6, RGTC1-E1, RGTC1-W9, RGTC1-W16, RGTC1-E17, RGTC1-E16) to estimate the two events: event E1 (7230-3015 BC) and event E2 (885-525 BC) (Figure. 6). The sinistral-oblique offset of the U3 pinch-out must be due to displacements in two seismic events: the second paleoearthquake event mentioned above, and the historical earthquake in 1854 that produced a 3 m displacement on the Ezhong footpath. Using the measured sinistral-oblique offset of the U3 pinch-out and the ages of samples within and overlying U3 (770-475 BC and 985-1155 AD), the sinistral-slip rate is estimated to be between 2.9±0.3 mm/a and 8.0±0.3 mm/a , and the throw rate is between 0.4±0.1 mm/and a1.1 ±0.1 mm/a.

4.3 Cuoa

There are three terraces at Cuoa village, all cut by the Ganzi-Yushu fault. T3 and T2 are only preserved on the west side of the river. The vertical dislocation between hanging wall and footwall

234 is 8m on the T3 terrace and 2-3 m on the T2 terrace, and the T3/T2 riser is offset in a sinistral
235 sense by about 80 m. The fault is exposed on the west side of the river, where it places Triassic
236 slate and metasandstone of the southwest (hanging wall) block over Quaternary sand and gravel of
237 the northeast (foot wall) block. The fault dips 68° toward 305° (Figure 7d).
238 The CATC1 trench was excavated in the T2 terrace near Cuoa township (Figure 7b), perpendicular
239 to a 2 m fault scarp. The hanging wall is composed primarily of bedrock on the southwestern side
240 of the fault, overlain by units U4 and U5 (Figure 8). The presence of resistant bedrock at the
241 hanging wall has allowed accumulation of at least two distinct sediment wedges in the footwall,
242 along with unit U3. The fault is expressed in both walls of the trench as a positive flower structure
243 with a general dip to the southwest, and five separate fault planes can be identified:
244
245 Fault F1 cuts unit U3 and appears to terminate at the base of U4 on the east wall of CATC1. On
246 the west wall, however, F1 terminates at the base of U3. Fault F2 cuts unit U3 and U4 on the east
247 wall, but only cuts unit U3 on the west wall. Fault F3is only visible at the east wall of CATC1. It
248 cuts unit U4 and wedge A, and appears to terminate at the base of U5.The fault is divided into two
249 branches within wedge A, leading to about 10-20 cm vertical offset of the top surface of wedge A.
250 Fault F4 cuts unit U4, wedge A and wedge B, and appears to terminate at the base of U5. Fault F5
251 cuts unit U4, wedge A and wedge B on the east wall, but on the west wall, it is covered by wedge
252 B. We infer that two paleoearthquake events are recorded in the CATC1 trench, both of which
253 post-date deposition of units U1, U2 and U3. We use OxCal 4.2.4 (Bronk Ramsey, 2013) by 6 ^{14}C
254 age (CATC1-W6, CATC1-E5, CATC1-E3, CATC1-W3, CATC1-W4, CATC1-E4) to estimate the
255 two events: event E1 (3580-2640 BC) and event E2 (2135-1510 BC) (Figure 9). The first event

involved faults F1 and F2, and formed wedge A between U1 and U3. Materials in the wedge appear to have been derived from U3 (Figure 10b). Samples from the upper portion of U3 and from wedge A indicate that the lower limit time on the first paleoearthquake is 3655-3515 BC and the upper limit time is 2780-2560 BC (Figure 8). Unit U4 was deposited after the first event. The second paleoearthquake event occurred after deposition of unit U4, and involved faults F4 and F5 (Figure 10c). Expressions of the second event are different on the two walls of the CATC1 trench. Slip on F3 appears to have resulted a suite dislocates in wedge A and slip on F2 appears to have resulted in wedge A slipping down between F2 and F4 on the east wall. The overlying layer U4 collapsed, allowing deposition of wedge B between F4 and F5. In contrast, F3 shows no signs of rupture in the second paleoearthquake on the west wall of the trench. Instead, F4 dislocated U4 and wedge B was formed above unit U4 in the hanging wall (Figure 10d). The upper and lower limit times for the second paleoearthquake are constrained by ^{14}C ages on wedge B of 1620-1435 BC and on U4 of 2210-1975 BC (Figure 8). The surface layer U5 was deposited after the second event, and yields a ^{14}C age of 1150-1275 AD (Figure 10e).

The epicenter of the M~8 Zhuqin-Ria earthquake in AD1320 is thought to be near to the CATC1 trench [Zhou et al., 1997]. The bulges and small scarps developed on the T2 surface at Cuoa (Figure 8d) may be related to this historical earthquake, which occurred after the deposition of U5. However, we do not see direct evidence of this earthquake in the trench.

Because of abundant ^{14}C samples from CATC1 on T2 and obvious offsets of the T2 surface, T2 is thus an extremely well-suited place to determine the fault slip rate. We use the sinistral offsets of

the T3/T2 riser and the T2 age to evaluate the sinistral-slip rate, and the throw rate is evaluated from the height of scarp on T2 and the T2 age. The sinistral and vertical offsets, as obtained from DGPS surveys, are 80 m and 2.5 m, respectively. If we use the age (6115-5970 BC) of sample CATC1-E4 (see Figures 7 and 8 for location) in unit U3 of CATC1 to approximate the T2 age, then the sinistral-slip rate and throw rate are 10±0.4 mm/a and 0.3±0.1 mm/a. Note that this is a minimum age for the T2 fill terrace, because the riser formed before any of the T2 deposits were load down, so this is maximum limiting slip rate.

4.4 Ria

Ria is located 30km to the northwest of Cuoa (Figure 2), and shows clear evidence of offset fill terraces (Figure 11). We obtained horizontal and vertical offsets from field surveys. The T3/T2 riser is sinistrally offset by about 80 m, similar to the offsets of T3 terrace margins located about 500m to the southeast (Figure 11). The T2/T1 riser is sinistrally offset by about 20 m. The vertical offsets of the T3 and T2 terrace treads are 10 m and 8 m, respectively. Wen et al. [2003] published an estimate Holocene slip rates of 12±8 mm/a in the horizontal and 1.2±0.2 mm/a in the vertical by T2 age.

5 Discussion

Our results provide clear evidence for late Quaternary oblique sinistral-thrust activity on the southeastern Ganzi-Yushu fault at rates of 8 to 11 mm/a in the horizontal and 0.3 to 1.1 mm/a in

298 the vertical. These slip rates provide important constraints on the applicability of different tectonic
299 models for the present-day deformation of the Tibetan Plateau. Block models have been suggested
300 that actively deforming regions are comprised of blocks or microplates. Most deformation occurs
301 along major blocking faults, with minor faulting but little internal deformation of the blocks
302 themselves. So this model has been advocated primarily by geologists who cite evidence for high
303 (10-30 mm/a) slip rate on the major strike-slip faults of Tibet [e.g. Avouac and Tapponnier, 1993].
304 On the contrary, continuum models are viewed as quasi-continuous, governed by the fluid-like
305 solid-state flow of a viscous material. This model has been proposed primarily by geophysicists
306 using laboratory measurements to contrain the ductile flow properties of Earth's lithosphere, its
307 strong outer, ~100 km thick surface layer, and construct dynamical models of continental
308 deformation [e.g., England and Molnar, 2005]. In this view, discrete slip in the brittle upper crust
309 occurs on many faults with roughly comparable slip rates.
310
311 For many of the large strike-slip faults within the Indo-Asian collision zone [e.g. Allen et al., 1991;
312 Van et al., 2002], slip rates determined geodetically are generally different to those reported using
313 reconstructions of offset landforms, and it is unclear if this discrepancy reflects true secular
314 variation in slip history, systematic errors in interpretation, or both. Even slip rates reported using
315 different reconstructions of offset landforms along the same fault are different. A major potential
316 source of uncertainty when assessing slip rates from offset fill terraces is the underlying
317 geomorphic model of terrace formation and abandonment that must be assumed [e.g., Zhang et al.,
318 2004; Cowgill, 2007]. One evolutionary model suggests that the erosion of flood plain and its
319 banks continues until the river begins to incise and new terraces are formed [Van et al., 2002].

320 According to this model, offset of a terrace riser only begins to accumulate once the lower terrace
321 is abandoned. An alternative model allows for differences in erosion pattern between the sides of
322 the river, in which case riser offsets may begin to accumulate after the upper terrace is abandoned.
323
324 Based on our field observations, we suggest that, at different sites along the Ganzi-Yushu fault,
325 different models are most suitable. At Shengkang, the T5/T3 riser cannot be eroded because of its
326 location away from the position of the river (Figure 12a, b). So we use the offset of the T5/T3 riser,
327 divided by the abandonment age of T5, to calculate the slip rate. We cannot, however, use the
328 same method to calculate the slip rate at Ria, because the risers are subject to erosion by the river
329 (Figure 12c, d). Assuming that the offsets could not begin to accumulate before the abandonment
330 of T2, we the offset of the T3/T2 riser, divided by the abandonment age of T2, to calculate the slip
331 rate. At Cuoa, the offsets have the same geometry with respect to the river as at Shengkang, but
332 we cannot use the same model, because the river geometries are different at these two sites. The
333 arc-shaped river at Cuoa has led to more erosion on the left side of the river (Figure 12e, f), so the
334 slip rate is obtained by dividing the offset of the T3/T2 riser by the abandonment age of T2.
335
336 Our results also place important constraints on the occurrence times of paleoearthquake events on
337 the southeastern segment of the Ganzi-Yushu fault. Our work demonstrates that two
338 paleoearthquake events are recorded in the trench at Renguo (Figure 13). We use OxCal 4.2.4
339 (Bronk Ramsey, 2009) to estimate the two events: event E1 (885-525 BC) and event E2
340 (7230-3015 BC). Based on our work on the Cuoa trench, there are also two paleoearthquake
341 events: event E1 (3580-2640 BC) and event E2 (2135-1510 BC). Considering that the distance

between Renguo and Cua is only 40 km and that there is no obvious step or discontinuity in the fault trace over this distance, we suggest that the faults between Rengou and Cua are likely to have similar rupture histories. If this is correct, then we can analyse earthquake occurrence times using paleoearthquakes from the two trench sites and historical earthquakes. Two documented historical earthquakes respectively occurred in 1320 AD and 1854 AD. Thus, while the data are limited, there does seem to be some evidence of clustering of large earthquakes along the southeastern Ganzi-Yushu fault (Figure 13).Three or four paleoearthquakes occurred during about 3000 years from 3580-2640 BC to 885-525 BC (yielding an approximate recurrence interval of ~1000 a), but there appear to have been no large earthquakes during the 2000 years from 885-525 BC to 1320 AD. Finally, two large historical earthquakes have happened in the past 630 years (Figure 13). This apparent clustering behavior has been observed on other large strike-slip fault systems, for example, Sieh [1989] discussed the clustering of earthquakes along the San Andreas Fault. Over the Holocene at least, there is no evidence for periodic earthquakes on the southeastern Ganzi-Yushu fault, and the occurrence of two large earthquakes since 1320 AD may indicate that the fault is currently in a phase of relative activity.

6 Conclusions

We have documented Quaternary activity on the Ganzi-Yushu fault, using a combination of field observations, photo and image interpretation, and trenching. The Ganzi-Yushu fault, which forms part of the boundary between the Qiangtang and Bayankala blocks, has been active in the latest Quaternary with an oblique sinistral-thrust sense of slip. More precise chronology and offset

363 measurements for the dominant sinistral strike-slip displacement suggest that sinistral strike-slip
364 rates may be 8-11mm/a. Apparent throw rates are typically ~1 mm/a. Our trench investigations
365 indicate that Holocene earthquakes on the southeastern segment of the Ganzi-Yushu fault show
366 some evidence for clustering of activity. From the past 5600 years, the fault appears to have
367 undergone two active periods separated by a period of relative quiescence. Our more precise slip
368 rates provide essential evidence in understanding the mechanism of the Bayan Har fault-block in
369 the India-Asia collision.
370
371 **Acknowledgements:**
372 This work has been funded by the central level, scientific research institutes for basic R & D
373 special fund business (IGCEA1416) and Yushu Earthquake Science Investigation of China
374 Earthquake Administration.
375

376 # References

377 Allen C R, Luo Z, Qian H, et al (1991). Field study of a highly active zone: the Xianshuihe fault of southwestern
378 China. *Geol. Soc. Am. Bull., 103,*1178-1199.
379 Avouac, J.-P., and P. Tapponnier (1993), Kinematicmodel of active deformation in central Asia, *Geophys.Res. Lett.,*
380 *20,* 895 – 898.
381 Bronk Ramsey, C. (2009). Bayesian analysis of radiocarbon dates. Radiocarbon, 51(1), 337-360.
382 Burchfiel, B. C., Z. Chen, Y. Liu, and L. H. Royden(1995), Tectonics of the Longmen Shan and adjacentregions,
383 *Int. Geol. Rev., 37,* 661 – 735.

Chen, L.C., H., Wang, Y.K. Ran, X.-Z. Sun, G.W. Su, J. Wang, X.B. Tan, Z.M. Li, and X.Q. Zhang (2010)， The Ms7.1 Yushu earthquake surface rupture and large historical earthquakes on the Garzê-Yushu Fault,*Chin. Sci. Bull., 55*(31), 3504-3509.

Chen, S., C. J. L.Wilson, Q. Deng, X. Zhao, and Z. Luo(1994), Active faulting and block movement associatedwith large earthquakes in the Min Shan andLongmen Mountains, northeastern Tibetan Plateau,*J. Geophys. Res., 99,* 24025 – 24038.

Chen, Y.T., 2010. The report of focal mechanism and rupture process of 2010. 4. 14 Yushu earthquake, Qinghai, China (the fourth edition). http://www.csi.ac.cn/manage/html/4028861611c5c2ba0111 c5c558b00001/ _content/10_04/17/1271488288058.html (in Chinese).

Clark, M. K., M. A. House, L. H. Royden, K. X.Whipple, B. C. Burchfiel, X. Zhang, and W. Tang(2005), Late Cenozoic uplift of southeastern Tibet,*Geology, 33,* 525 – 528.

Cowgill, E. (2007), Impact of riser reconstructions onestimation of secular variation in rates of strike-slipfaulting: Revisiting the Cherchen River site alongthe AltynTagh Fault, NW China, *Earth Planet. Sci.Lett.,* 254, 239 - 255.

Densmore, A. L., M. A. Ellis, Y. Li, R. J. Zhou, G. S. Hancock, and N. Richardon (2007), Active tectonics of the Beichuan and Pengguan faults at the eastern margin of the Tibetan Plateau, *Tectonics, 26,*TC4005, doi:10.1029/2006TC001987.

Dewey, J. F., W.C. Pitman, W.B.F. Ryan, and J. Bonnin (1973), Plate tectonics and the evolution of the Alpine system, *Geol. Soc. Am. Bull.,* 84, 3137-3180.

England, P., and D. McKenzie (1982), A thin viscoussheet model for continental deformation, *Geophys.J. R. Astron. Soc., 70,* 295 – 321.

England, P., and G. Houseman (1986), Finite straincalculations of continental deformation: 2. Comparisonwith the

India-Asia Collision, *J. Geophys.Res., 91,* 3664 – 3676.

England, P., and P. Molnar (2005), Late Quaternary todecadal velocity fields in Asia, *J. Geophys. Res.,110,* B12401, doi:10.1029/2004JB003541.

Forman, S. L. (1989), Applications and limitations of thermoluminescence to date Quaternary sediments, *Quatern. Int., 1,* 47-59.

Gan, W.J., P.Z. Zhang, Z.K. Shen, Z.J. Niu, M. Wang, Y.G. Wan, D.M. Zhou, and J. Cheng (2007), Present-day crustal motion wihtin the Tibetan Plateau inferred from GPS measurements, *J. Geophys.Res., 121,*B08416, doi:10.1029/2005JB004120.

He, H.L., Ran, H.L., Ikada, Y.,(2006). Uniform strike-slip rate along the Xianshuihe-Xiaojiang fault system and its implications for active tectonics in southeastern Tibet. *ACTA GeologicaSinica*, 2: 376-386.

Kirby, E., K. X. Whipple, B. C. Burchfiel, W. Tang,G. Berger, Z. Sun, and Z. Chen (2000), Neotectonicsof the Min Shan, China: Implications formechanisms driving Quaternary deformation alongthe eastern margin of the Tibetan Plateau,*Bull.Geol. Soc. Am., 112,* 375 – 393.

Kirby, E., K. X. Whipple, W. Tang, and Z. Chen (2003), Distribution of active rock uplift alongthe eastern margin of the Tibetan Plateau: Inferencesfrom bedrock channel longitudinal profiles,*J. Geophys. Res., 108*(B4), 2217, doi:10.1029/2001JB000861.

Kirby, E., P. W. Reiners, M. A. Krol, K. X. Whipple,K. V. Hodges, K. A. Farley, W. Tang, and Z. Chen(2002), Late Cenozoic evolution of the eastern marginof the Tibetan Plateau: Inferences from40Ar/39Ar and (U-Th)/He thermochronology, *Tectonics*,*21*(1), 1001, doi:10.1029/2000TC001246

Li, C.-Y., J.-Z. Pang, and Z.-Q. Zhang (2012), Characteristics, geometry, and segmentation of the surface rupture associated with the 14 April 2010 Yushu earthquake, eastern Tibet, China, *Bull.Geol. Soc. Am., 102*(4), 1618-1638.

Li, M.F, C.Q.Xing, C.X.Cai, W.X.Guo, S.X.Wu, Z.Z.Yuan, Y.Q.Meng, D.L.Tu, R.B.Zhang and R.J. Zhou (1995), Research on activity of Yushu fault. *Seismology and Geology*, 17(3): 218-224 (in Chinese with English abstract).

McCalpin, J.P. (1996),Paleoseismology. Elsevier, New York.

Meade, B. J. (2007), Present-day kinematics at the India-Asia collision zone, *Geology, 35*, 81 – 84.

Mêriaux, A. S., F. J. Ryerson, P. Tapponnier, J. van derWoerd, R. C. Finkel, X. Xu, Z. Xu, and M. W.Caffee (2004), Rapid slip along the central AltynTagh Fault: Morphochronologic evidence fromCherchen He and SulamuTagh, *J. Geophys. Res.,109*, B06401, doi:10.1029/2003JB002558.

Molnar, P., and P. Tapponnier (1975), Cenozoic tectonicsof Asia: Effects of a continental collision,*Science*, *189*, 419 -426.

Molnar, P., and P. Tapponnier (1978), Active tectonics of Tibet, *J. Geophys. Res., 83,* 5361-5375.

Peltzer, G., and F. Saucier (1996), Present-day kinematics of Asia derived from geological fault rates,*J. Geophys. Res., 101*, 27,943 - 27,956.

Peng, H., Ma, X.M., Bai, J.Q., Du, D.P., (2006). Characteristics of quaternary activities of the Ganzê-Yushu fault zone. *Journal of Geomoechanics*, 12(3): 295-304.

Seih, K., M. Stuiver and D. Brillinger (1989), A more precise chronology of earthquakes produced by the San Andreas Fault in southern California. *J. Geophys. Res., 94*,603-623.

Shen, Z.K., J.N. Lü, M. Wang, and R. Bürgmann(2005), Contemporary crustal deformation aroundthe southeast borderland of the Tibetan Plateau,*J. Geophys. Res., 110,* B11409, doi:10.1029/2004JB003421.

Tapponnier, P., Z.Q. Xu, F. Roger, B. Meyer, N. Arnaud,G.Wittlinger, and J.-S. Yang (2001), Oblique stepwiserise and growth of the Tibet Plateau, *Science*, *294*,1671-1677.

Thatcher, W. (2007), Microplate model for the present-daydeformation of Tibet, *J. Geophys. Res., 112*,B01401,

450 doi:10.1029/2005JB004244.

451 USGS. (2010), Magnitude 6.9 Southern Qihai, China.http://earthquake.usgs.gov/earthquakes/recenteqsww

452 /Quakes/us2010vacp.php

453 Van der Woerd J P, Tapponnier F J, Ryerson, et al. (2002). Uniform postglacial slip-rate along the central 600 km

454 of the Kunlun Fault (Tibet), from ^{26}Al, ^{10}Be, and ^{14}C dating of riser offsets, and climatic origin of the

455 regional morphology. G*eophys. J. In.t, 148*, 356-388.

456 Wang, Q., P.Z. Zhang, J. T. Freymuller, R. Bilham, K. M. Larson, X.-A. Lai, X.-Z. You, Z.-J. Niu, J.-C. Wu, Y.-X.

457 Li, J.-N. Liu, Z.-Q. Yang, and Q.-Z. Chen (2001), Present-day crustal deformation in China constrained by

458 global positioning system measurements, *Science, 294*, 574-577.

459 Wang, Y. Z. (2009). Continental Deformation Models and Their Application to EasternTibetan Plateau, *Doctoral*

460 *dissertation* , Institute of Geology, China Earthquake Administration,Beijing.

461 Wen, X.Z, Xu, X.W.,Zheng, R.Z., Xie, Y.Q., Wan, C., (2003). Average slip-rate and recent large earthquake

462 ruptures along the Garzê-Yushufault.Science in China (Series D), 46(Suppl): 276-288.

463 Xu, G., and P. J. J. Kamp (2000), Tectonics anddenudation adjacent to the Xianshuihe fault, easternTibetan Plateau:

464 Constraints from fissiontrackthermochronology, *J. Geophys. Res., 105*,19231 – 19251.

465 Xu, X.W., X.B. Tan, G.D. Wu, J.B. Chen, J. Shen, W. Fang, and H.P. Song. (2011). Surface rupture features of the

466 2008 Yutian Ms7.3 earthquake and its tectonic nature. *Seismology and Geology*, 33(2): 462-471.

467 Xu, X.W. (2000), Scientific investigation of Mani earthquake in the north Tibet, in Y*earbook of China Earthquake*

468 *Research*, pp.327-329, China Earthquake Press, Beijing.

469 Xu, X.W., W.B. Chen, W.T. Ma, G.H., Yu and G.H. Chen. (2002). Surface rupture of the Kunlunshan earthquake

470 (Ms8.1), northern Tibetan Plateau, China. *Seimological Research Letters*. 73(6): 884-892.

471 Xu, X.W., X.Z Wen, G.H. Yu, G.H. Chen, Y. Klinger, J. Hubbard and J. Shaw. (2009). Coseismic revers- and

oblique-slip surface faulting generated by the 2008 Mw7.9 Wenchuan earthquake, China. *Geology*, 37(6): 515-518.

Zhang, P.Z., Q.D.Deng, G.M.Zhang (2003),Active tectonics blocks and strong earthquakes in the continent of China. *Science in China (Series D)*, 46(Suppl): 13-24.

Zhang, P.Z., et al. (2004), Continuous deformation ofthe Tibetan Plateau from global positioning systemdata, *Geology, 32*, 809-812.

Zhou, R.J., S.H.Ma , C.X.Cai (1996), Late Quaternary active features of the Ganzi-Yushu fault zone. *Earthquake Research in China*, 12(4): 250-260.

Zhou, R. J., X. Z. Wen, C. X. Chai, S. H. Ma (1997), Recent earthquakes and assessment of seismic tendency on the Ganzi-Yushu fault zone. *Seismology and Geology,* 19(2): 115-124.

Figure captions

Figure 1. Regional seismotectonics and historical earthquakes of the study region. A, Simplified map of major tectonic boundaries and Tertiary faults in Tibet (after Tapponnier et al., 2001). Bold black lines are major faults and localized shear zones (megathrust or strike-slip) with largest finite offsets, dashed where uncertain. Thin red lines are crustal thrusts. Red circles are the four largest earthquakes (M_w>7.0) during the last two decades in Tibet. Pentagram is the 2010 M_w6.9 Yushu earthquake. The black rectangle indicates the location of panel B. B, faults, major river systems, and areas of Quaternary deposition in the east-central Tibetan Plateau. The fault locationsare modified from Deng [2007].The 2010 Yushu earthquake focal mechanism was extracted from the CDSN [Chen, 2010], USGS and Harvard [USGS, 2010] catalogues.

493

494 **Figure 2.** A, historical earthquake surface ruptures along the Ganzi-Yushu fault. Surface ruptures
495 of the 2010 M_w 6.9 Yushu earthquake from Chen et al. [2010] and Li et al. [2012]. Surface
496 ruptures of the 1896, 1866 and 1854 earthquakes from Wen et al. [2003]. B, strike-slip rates along
497 the Ganzi-Yushu fault. Black, blue and purple circles are geological estimates of strike-slip rates
498 from Zhou et al. [1996], Wen et al. [2003] and Peng et al. [2006], respectively. Black, white, red
499 and blue lines with shadows are strike-slip rates and errors estimated from GPS surveys[Wang et
500 al., 2001; Shen et al., 2005; Gan et al., 2007; Wang, 2009]

501

502 **Figure 3.** Map of offset fill terraces at Shengkang. A, the original stereoscopic pair aerial
503 photograph. B, geomorphic interpretation of the aerial photograph. Yellow, green and brown areas
504 are T3, T4 and T5 surfaces. Blue area is the present-day river. Red square is the location of the TL
505 age sample from Wen et al. [2003]. Black line is the location of topographic profile in C. C,
506 topographic profile extracted from a 20 m DEM constructed from 1:50,000 maps.

507

508 **Figure 4.** Tectonic landforms and evidence of fault activity at Renguo. A, the original aerial
509 photograph. B, interpreted photograph showing the locations of panels C-F. C, oblique photograph
510 of the fault scarp; see the location in panel B.View to south. The location of the Renguo trenches
511 is shown in yellow. D,oblique photograph of the sag pond. Dashed red lines show the uncertain
512 fault trace; see the location in panel B. View to southwest. E, contour map near the trench (0.2 m
513 contour interval), obtained from a differential GPS measuring system. The fault scarp is about
514 1-1.5 m high; see the location in panel B. F, displacementof the footpath in Ezhong village. View

to south; see the location in panel B.

Figure 5. Trench site on the Ganzi-Yushu fault at Renguo. See figure 4 for location. A, log of west wall of Renguo trench 1 (RGTC1). B, log of east wall of RGTC1. C, log of south wall of Renguo trench 2 (RGTC2). D, log of north wall of RGTC2. Black lines separate units 1-4. See Table 1 for description of units. Faults F1-F4 are shown by red lines. Black triangles show locations of ^{14}C samples. Calibrated ages and sample numbers (Table 2) are shown in bold type. E, sketch map of U3 offsets. Grey area is U3, yellow area is the fault zone.

Figure 6. Results of OxCal analysis of radiocarbon dates from the trenching site. Lines with no fill are prior probability distributions, and solid curves are posterior distributions after OxCal analysis. Phases are summed probability for units with multiple radiocarbon dates.

Figure 7. Evidence for fault activity at Cuoa. A, the original stereoscopic pair aerial photograph. B, geomorphic interpretation of aerial photograph. Yellow to pale green shades represent T0-T3 terrace surfaces. Black rectangle is the location of trench. Red line indicates the fault traces. Dashed white lines indicate the T3/T2 riser, which is offset sinistrally by ~80m. C, overview of the site, looking northwest. See location and orientation in panel B. D, close-up photograph of the fault exposed in the T2/T0 riser. Bold red line is the fault, and yellow line is the top of Triassic bedrock.Fault dip direction and dip angle are shown in bold type.

Figure 8. Trench site on the Ganzi-Yushu fault at Cuoa. See Figure 7 for location. A, photo of

west wall of Cuoa trench 1 (CATC1). B, log of west wall of Cuoa trench 1 (CATC1). C, photo of east wall of Cuoa trench 1 (CATC1). D, log of east wall of CATC1. Black lines separate units 1-5. See Table 3 for description of units. Faults F1-F5 shown by red lines. Black triangles show locations of ^{14}C samples. Calibration ages and sample numbers are shown in bold type.

Figure 9. Results of OxCal analysis of radiocarbon dates from the trenching site. Lines with no fill are prior probability distributions, and solid curves are posterior distributions after OxCal analysis. Phases are summed probability for units with multiple radiocarbon dates.

Figure 10. Interpretation of paleoearthquakes in the CATC1 trench. A, the original status of the trench. B, the status after the first event. C, the status before the second event. D, the status after the second event. E, the present status of the trench. Colors represent different units. Black lines separate units 1-5. See Table 3 for description of units. Faults F1-F5 shown by red lines.

Figure 11. Evidence for fault activity at Ria. A,aerial photograph of the fault trace and offset fill terraces.B, interpreted photograph showing the terrace treads and the fault trace (red line). Dashed white lines are the terrace risers. Offsets of the risers are shown in white bold type..

Figure 12. Possible terrace evolution models at the different sites discussed in this paper. A, the original landscape at Shengkang. B, the present-day landscape at Shengkang. Red box indicates the location of the measured riser offset. C, the original landscape at Ria. D, the present-day landscape at Ria. Grey box is the eroded part of the upper terrace, which reduces the preserved

559 riser offset. Tan box is a part of the upper terrace which may also be eroded. E, the original
560 landscape at Cuoa. F, the present-day landscape at Cuoa. Note the arcuate path of the river and
561 erosion of the terrace riser on the right and left banks.
562
563 **Figure 13.** Occurrence times of pre-historical (black with arrows) and historical (dark grey)
564 earthquakes, and inferred active periods (light grey shading) of the southeastern segment of the
565 Ganzi-Yushu fault. The AD1320 event of Cuoa is inferred, because we lack direct
566 paleoseimological evidence of the earthquake at that site.
567

Table1
Click here to download Table: Table 1.docx

Table 1. Lithologic Units in RenguoTrench

Unit	Description
U1-1	Grey-yellow coarse gravel layer, dominated by gravel and cobbles with a diameter of 5-20 cm, with rare clasts over 20 cm. The gravel is poorly sorted and is slightly rounded. In some areas the stratum is dark grey when freshly exposed and becomes grey-white when dry.
U1-2	Grey gravel layer. The mean clast diameter is about 5 cm, with rare clasts over 10 cm.
U2	Grey fine gravel layer with darker color than U1-2. The mean clastdiameter is 1-3 cm.
U3	Grey to brown fine gravel layer, with mean clast size of5cm.This stratum in the west wall of RGTC1 is darker than the east. It only appears in the hanging wall of the east wall of RGTC1. The stratum thins from west to east in RGTC2.
U4-1	Yellow clay layer (cultural layer).The stratum has low gravel content and the mean gravel diameter is 3cm.A lot of charcoal derived from burned straw is distributed within this layer.
U4-2	Brown sandy clay layer which forms the surface soil and subsoil. The layer contains rare gravel clasts with diameter of 1-3cm.
Wedge A	Grey gravel layer. The mean clast diameter is about 5 cm, with rare clasts over 10cm. Materials in the wedge are similar to those from U1-1, but more loose.
Wedge B	Grey gravel layer. The mean clast diameter is about 10 cm, with rare clasts over 20 cm. There is obvious human remodeling in this layer. Materials in the wedge are similar to those from U4-1, but are coarser-grained.

.

Table 2. Radiocarbon Samples and Analytical Results

Sample	Material	Radiocarbon Age	13C/12C Ratio	2α Calendar Age
CATC1-E3	Charcoal	3710±40 BP	-23.8‰	2270-2255 BC (0.8%) 2210-1975 BC (94.6%)
CATC1-E4	Charcoal	7160±50 BP	-23.9‰	6205-6190 BC (1.1%) 6185-6140 BC (2.8%) 6115-5970 BC (85.9%) 5955-5915 BC (5.6%)
CATC1-E5	Charcoal	3250±40 BP	-24.3‰	1620-1435 BC
CATC1-W3	Charcoal	4090±40 BP	-24.2‰	2870-2800 BC (19.3%) 2780-2560 BC (69.2%) 2535-2490 BC (6.9%)
CATC1-W4	Charcoal	4790±40 BP	-24.5‰	3655-3515 BC (92.7%) 3410-3405 BC (0.5%) 3400-3380 BC (2.2%)
CATC1-W6	Charcoal	830±40 BP	-24.8‰	1050-1085 AD (4.3%) 1150-1275 AD (91.1%)
RGTC1-E1	Charcoal	2470±30 BP	-23.0‰	770-475 BC (92.4%) 465-450 BC (1.2%) 445-430 BC (1.8%)
RGTC1-E14	Charcoal	990±40 BP	-23.2‰	985-1155 AD
RGTC1-E15	Charcoal	1030±30 BP	-22.2‰	900-920 AD (2.8%) 960-1045 AD (91.9%) 1105-1120 AD (0.7%)
RGTC1-E16	Charcoal	13390±50 BP	-25.3‰	14340-13960 BC
RGTC1-E17	Charcoal	8310±40 BP	-23.7‰	7500-7250 BC (90.5%) 7230-7190 BC (4.8%)
RGTC1-W6	Charcoal	960±30 BP	-24.4‰	1020-1155 AD
RGTC1-W9	Charcoal	2670±40 BP	-21.4‰	905-795 BC
RGTC2-N1	Charcoal	2710±40 BP	-21.6‰	930-800 BC
RGTC2-S2	Charcoal	3450±40 BP	-22.1‰	1885-1665 BC
RGTC1-W16	Charcoal	4330±40 BP	-21.9‰	3085-3065 BC (3.4%) 3030-2885 BC (92.0%)

Note: All sample preparation and analyses were done by Beta Analytic Inc. All samples were analyzed using accelerator mass spectrometry. All of raw radiocarbon ages are calibrated by OxCal 4.2.4 (Bronk Ramsey, 2009). The calibration calculates probability distributions for raw radiocarbon ages with associated uncertainties (reported by the lab facility). Radiocarbon ages BP relative to 1950. All samples typically undergo the acid–alkali–acid (AAA) method before radiocarbon dating.

Table 3. Lithologic Units in Cuoa Trench

Unit	Description
U1	Cyan upper Triassic metasandstone.
U2	Brown coarse gravel layer, with some clay in the matrix. The mean gravel diameter is about 10-20 cm, with some finer grains of 2-5 cm.
U3	Black clay layer, with some fine gravel and mica fragments. The mean grain size of the gravel is 2-3 cm, with rare grains to 10 cm.
U4	Brown clay layer, with some fine gravel with a diameter of 1-2 cm.
U5	Brown clay layer (surface layer),with some fine gravel. The diameter of the gravel is about 2-5 cm.
Wedge A	Grey clay wedge. The wedge contains some fine gravel with a mean diameter of about 2-3 cm. Materials in the wedge were similar to those from U3.
Wedge B	Light brown clay and fine gravel wedge. The grain size of the fine gravel is 3-5 cm. Materials in the wedge were very similar to those in U5.

Figure1

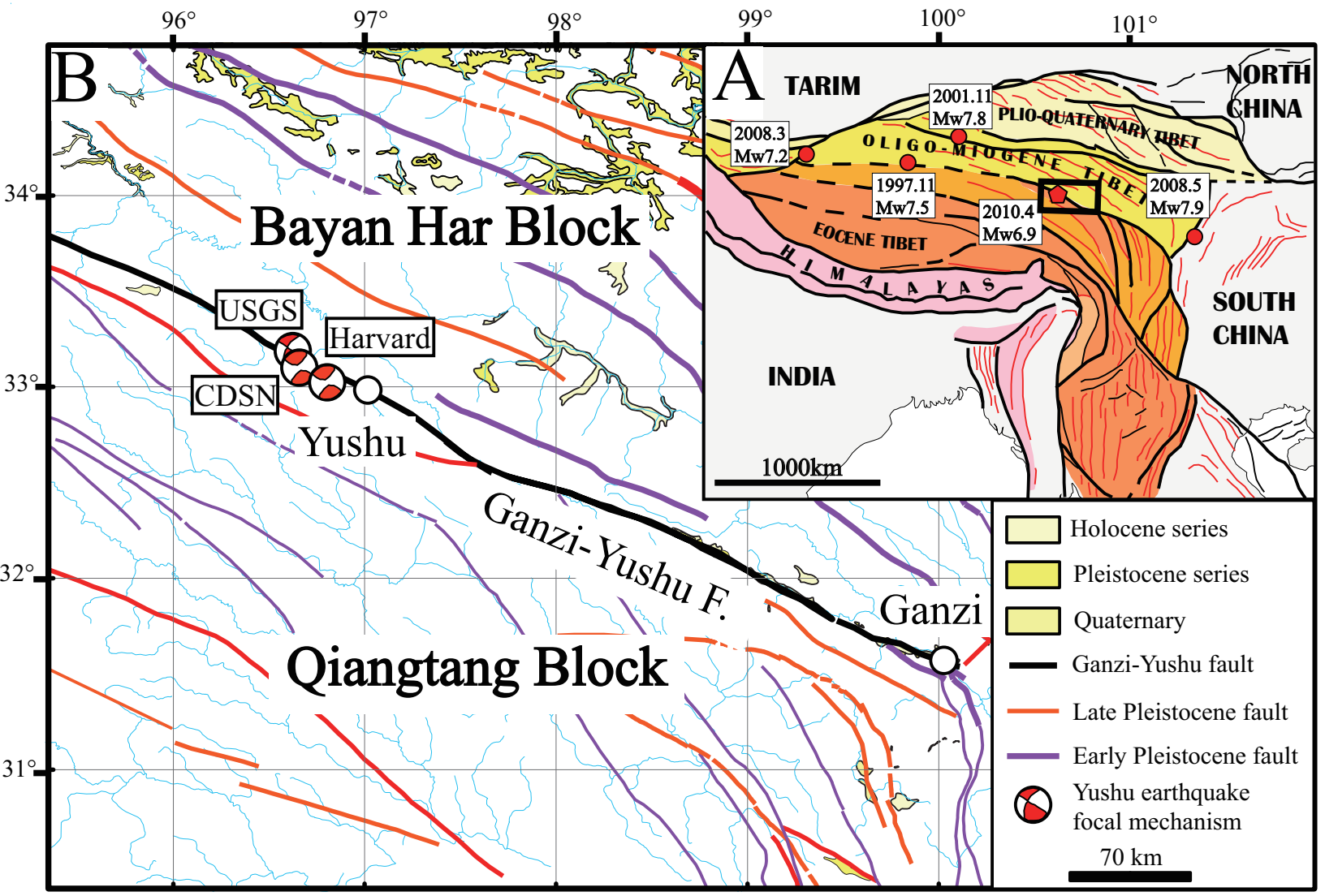
96°
97°
98°
99°
100°
101°
34°
33°
32°
31°
B
Bayan Har Block
USGS
Harvard
CDSN
Yushu
Ganzi-Yushu F.
Ganzi
Qiangtang Block
A
TARIM
NORTH CHINA
2001.11 Mw7.8
2008.3 Mw7.2
PLIO-QUATERNARY TIBET
OLIGO-MIOGENE TIBET
1997.11 Mw7.5
2010.4 Mw6.9
2008.5 Mw7.9
EOCENE TIBET
HIMALAYAS
SOUTH CHINA
INDIA
1000km
Holocene series
Pleistocene series
Quaternary
Ganzi-Yushu fault
Late Pleistocene fault
Early Pleistocene fault
Yushu earthquake focal mechanism
70 km

Figure2

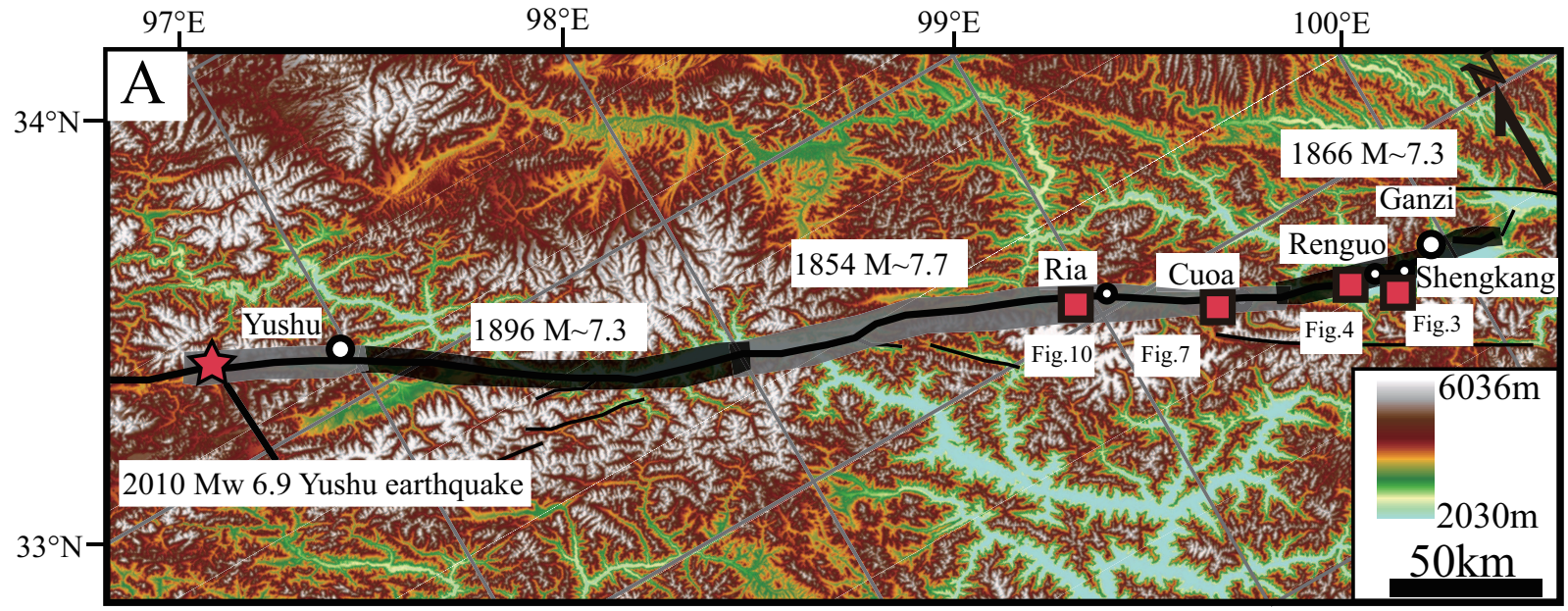
97°E
98°E
99°E
100°E
34°N
33°N
A
1866 M~7.3
Ganzi
Renguo
Shengkang
1854 M~7.7
Ria
Cuoa
Yushu
1896 M~7.3
Fig.4
Fig.3
Fig.10
Fig.7
2010 Mw 6.9 Yushu earthquake
6036m
2030m
50km

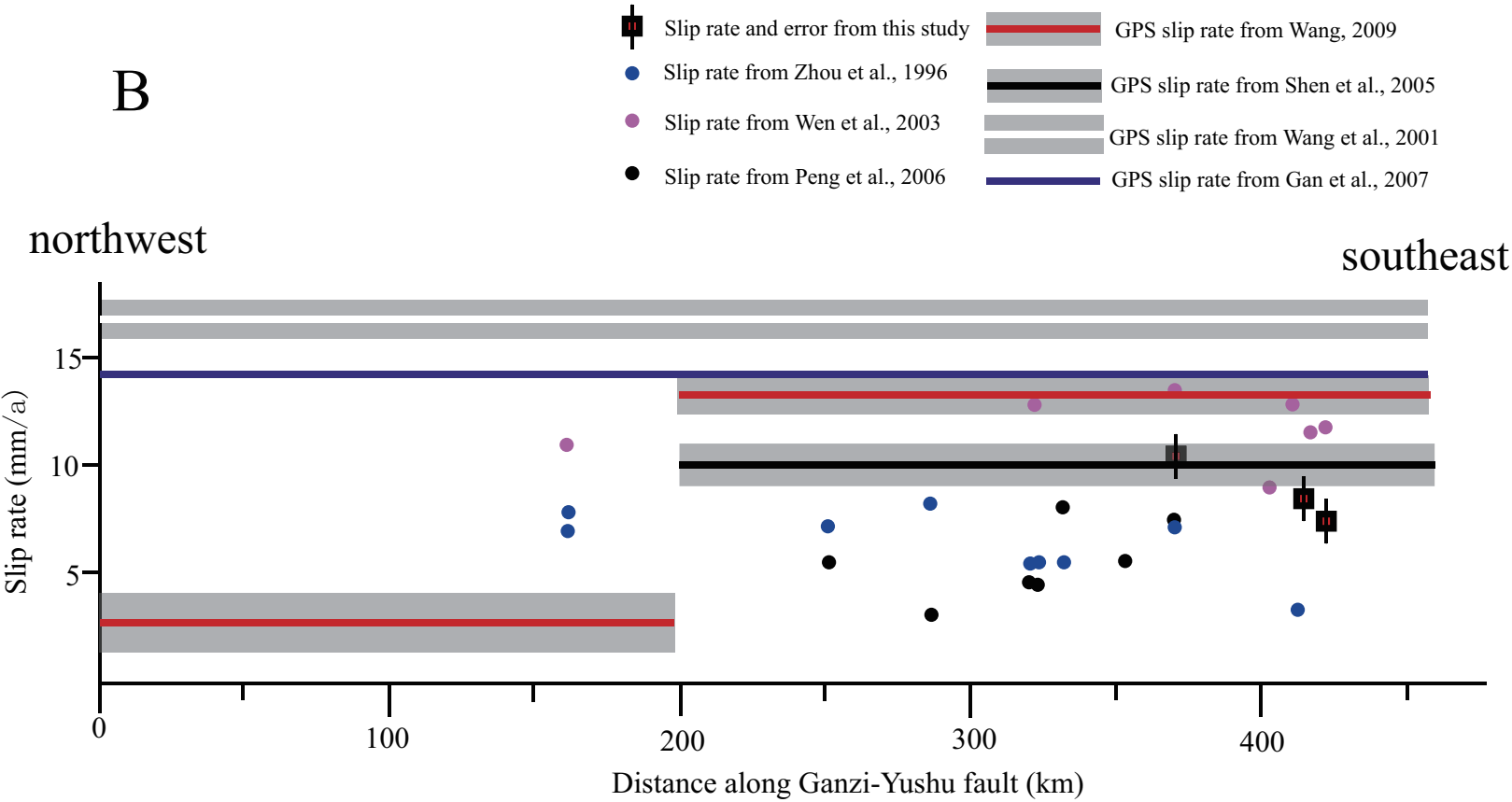
B
Slip rate and error from this study
Slip rate from Zhou et al., 1996
Slip rate from Wen et al., 2003
Slip rate from Peng et al., 2006
GPS slip rate from Wang, 2009
GPS slip rate from Shen et al., 2005
GPS slip rate from Wang et al., 2001
GPS slip rate from Gan et al., 2007
northwest
southeast
Slip rate (mm/a)
15
10
5
0
100
200
300
400
Distance along Ganzi-Yushu fault (km)

Figure3

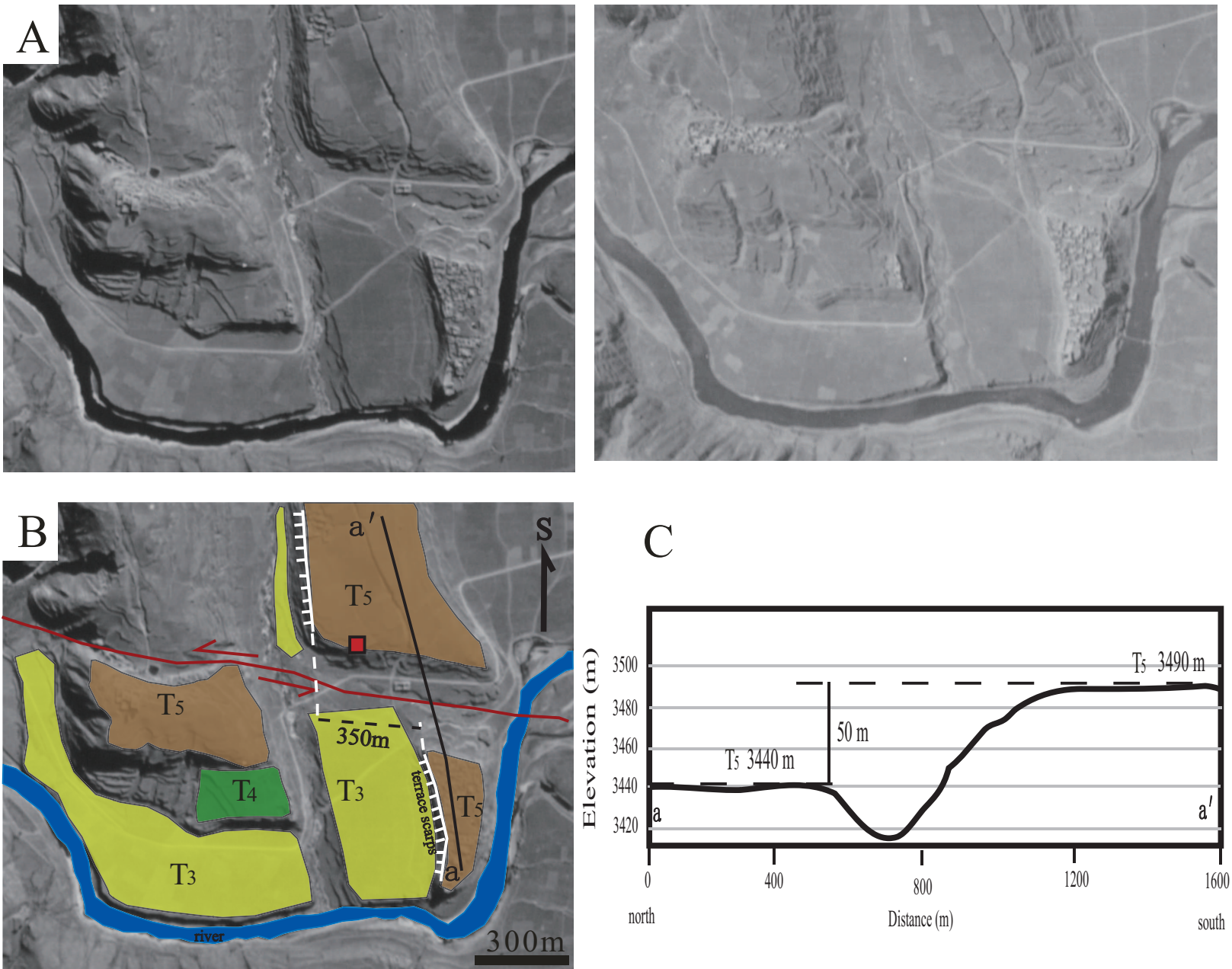
A
B
a′
S
T5
T5
350m
T4
T3
terrace scarps
T5
a
T3
river
300m
C
Elevation (m)
3500
3480
3460
3440
3420
T5 3490 m
50 m
T5 3440 m
a
a′
0
400
800
1200
1600
north
Distance (m)
south

Figure4

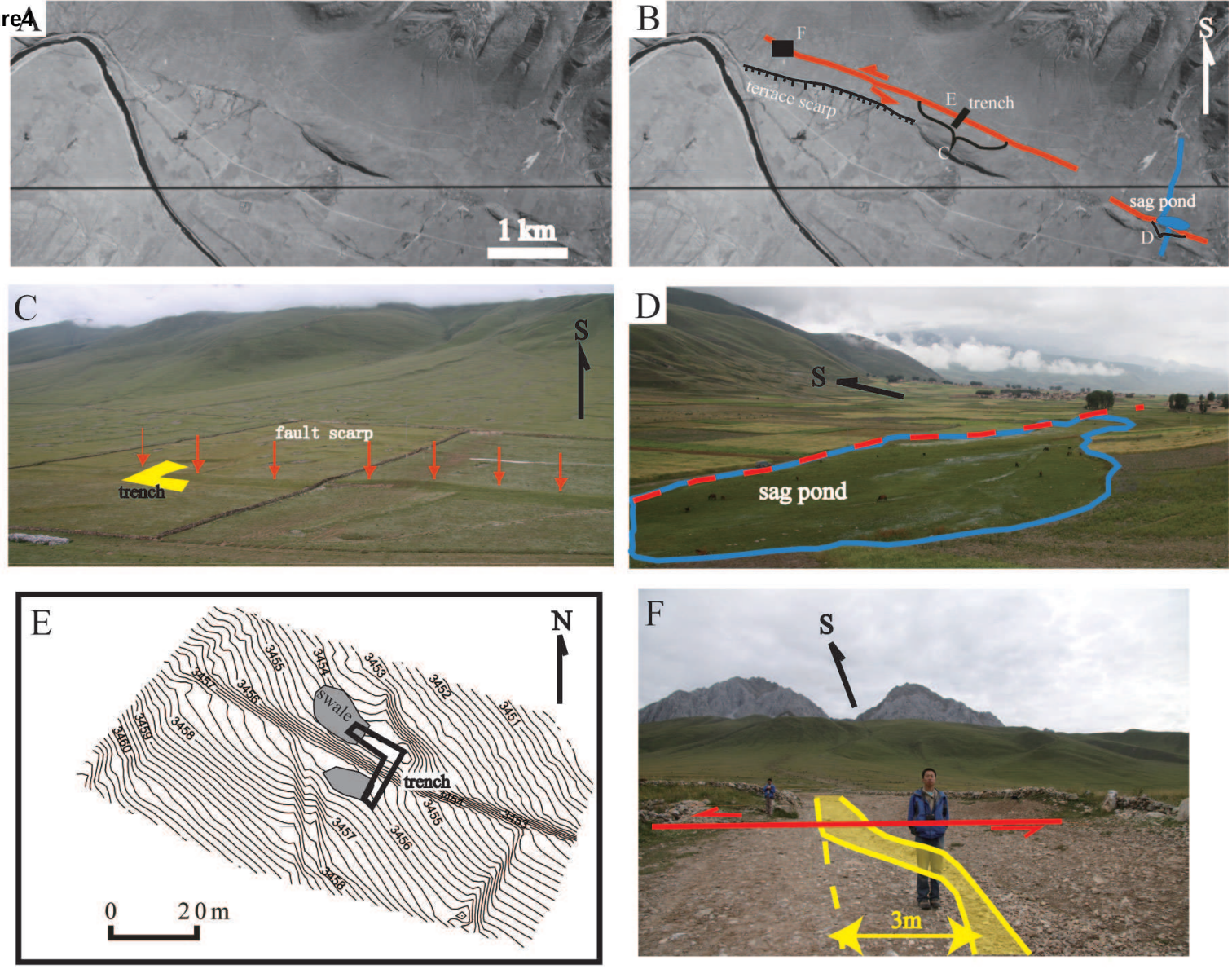

Figure 4. Tectonic landforms and evidence of fault activity at Renguo. A, the originalaerial photograph.B, interpreted photograph showing the locations of panels C-F. C, oblique photograph of the fault scarp; see the location in panel B.View to south. The location of the Renguo trenches is shown in yellow. D,oblique photograph of the sag pond. Dashed red lines show the uncertain fault trace; see the location in panel B. View to southwest. E, contour map near the trench (0.2 m contour interval), obtained from a differential GPS measuring system. The fault scarp is about 1-1.5 m high; see the location in panel B. F, displacementof the footpath in Ezhong village. View to south; see the location in panel B.

Figure5

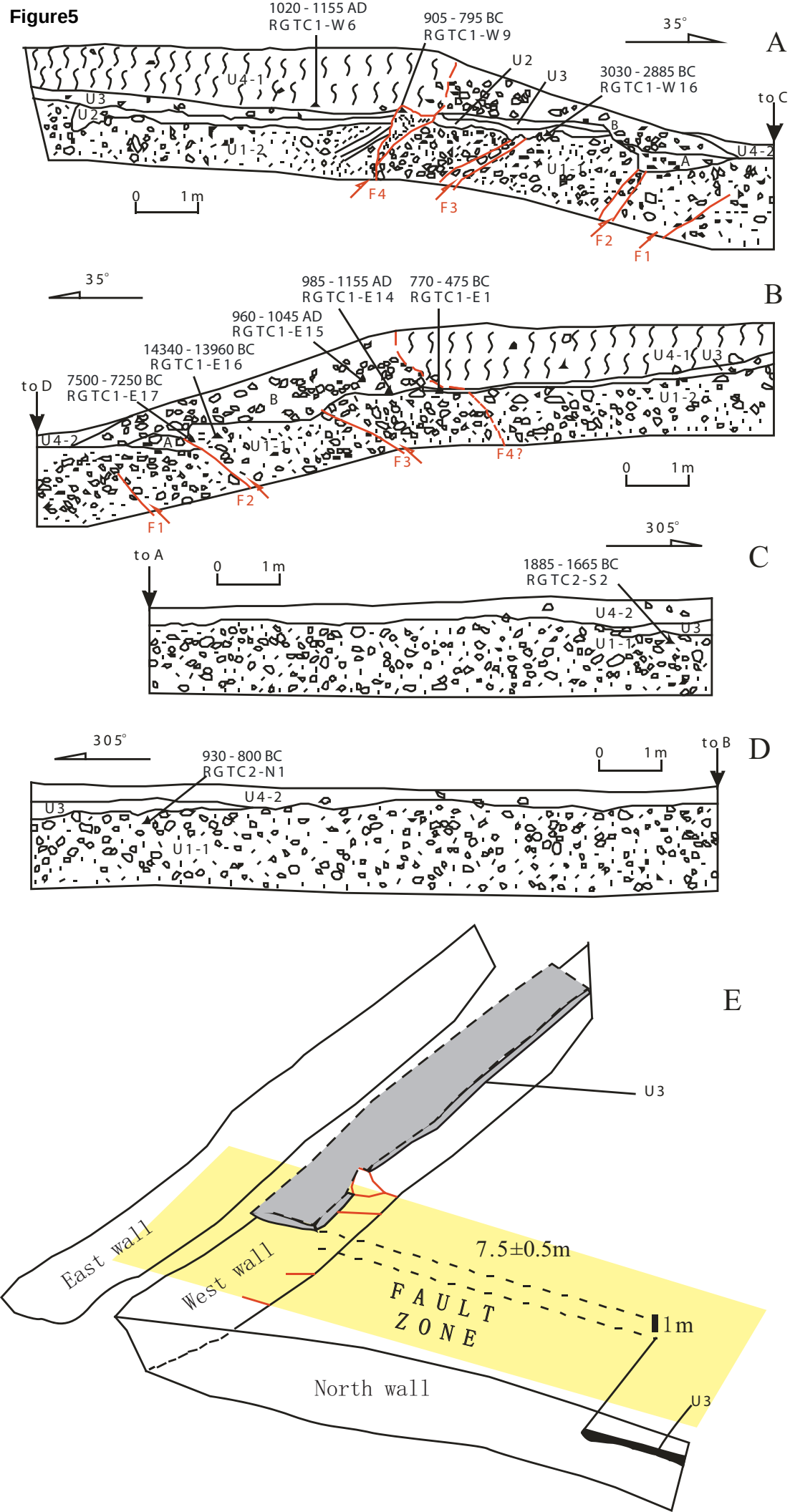
A
1020 - 1155 AD
RGTC1-W6
905 - 795 BC
RGTC1-W9
35°
U2
U3
3030 - 2885 BC
RGTC1-W16
to C
U4-1
U3
U2
U1-2
B
U1-1
A
U4-2
0 1m
F4
F3
F2
F1
B
35°
985 - 1155 AD
RGTC1-E14
770 - 475 BC
RGTC1-E1
960 - 1045 AD
RGTC1-E15
14340 - 13960 BC
RGTC1-E16
U4-1
U3
to D
7500 - 7250 BC
RGTC1-E17
U1-2
B
U4-2
A
U1-1
F3
F4?
0 1m
F2
F1
C
305°
to A
0 1m
1885 - 1665 BC
RGTC2-S2
U4-2
U3
U1-1
D
305°
930 - 800 BC
RGTC2-N1
0 1m
to B
U3
U4-2
U1-1
E
U3
East wall
West wall
7.5±0.5m
FAULT
ZONE
1m
North wall
U3

Figure6

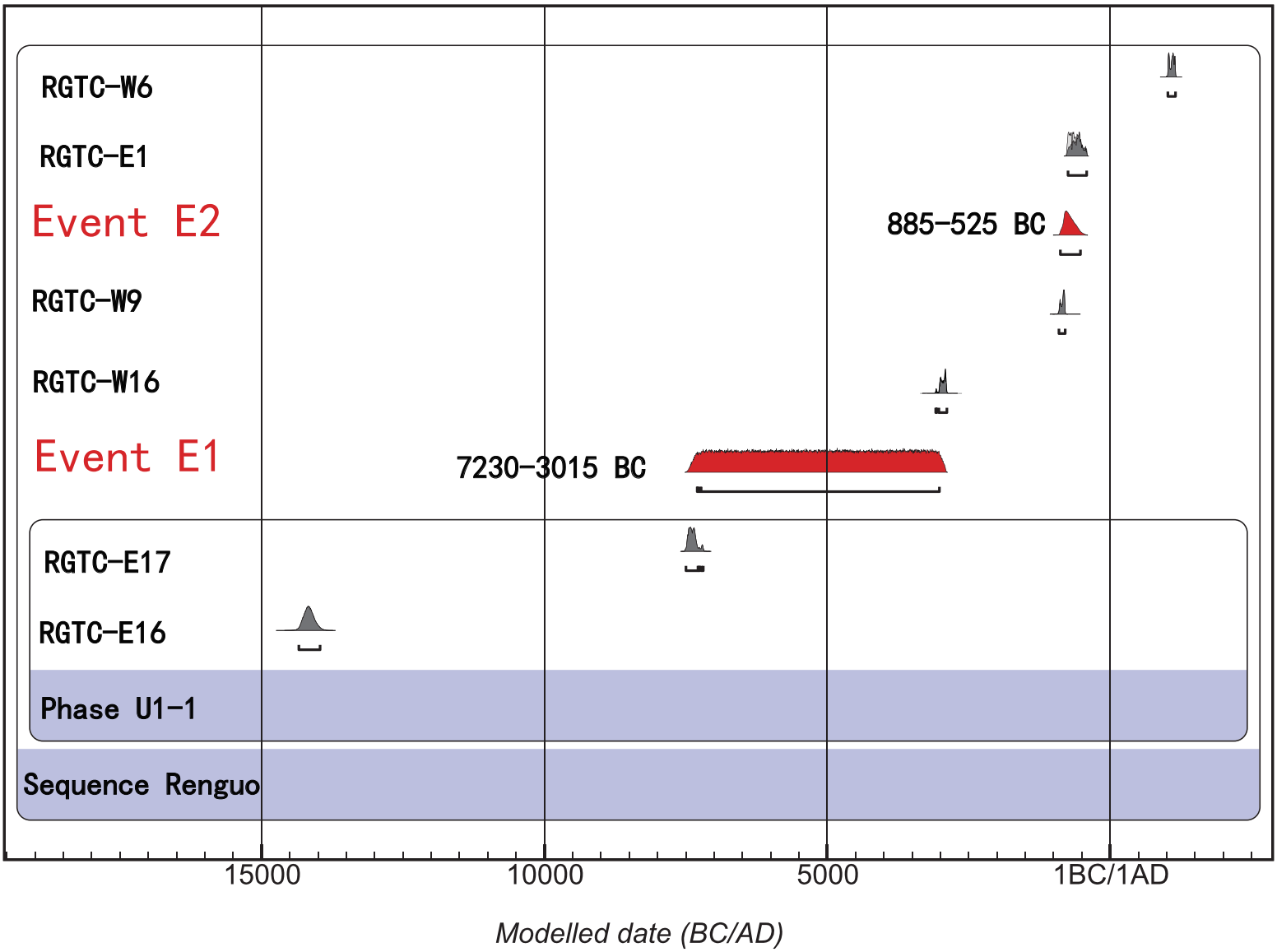
RGTC-W6
RGTC-E1
Event E2
885-525 BC
RGTC-W9
RGTC-W16
Event E1
7230-3015 BC
RGTC-E17
RGTC-E16
Phase U1-1
Sequence Renguo
15000
10000
5000
1BC/1AD
Modelled date (BC/AD)

Figure7

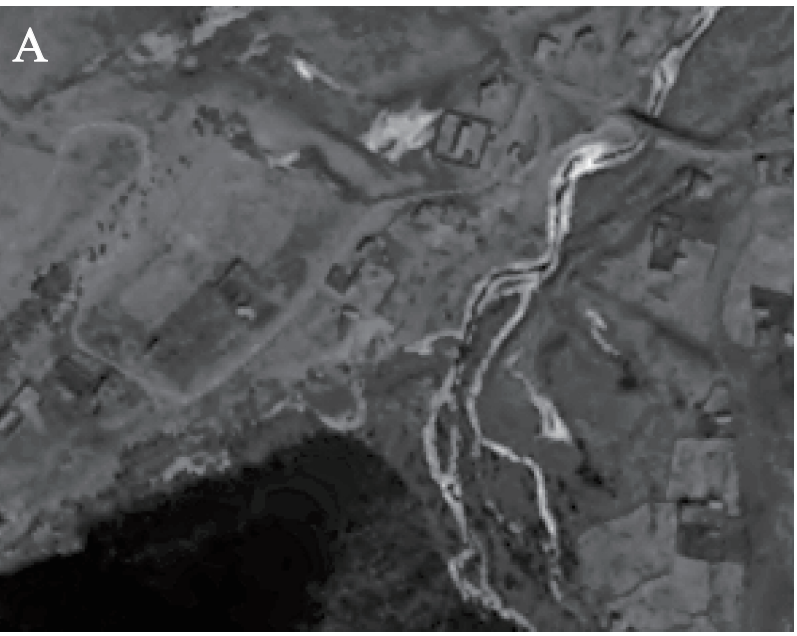
A

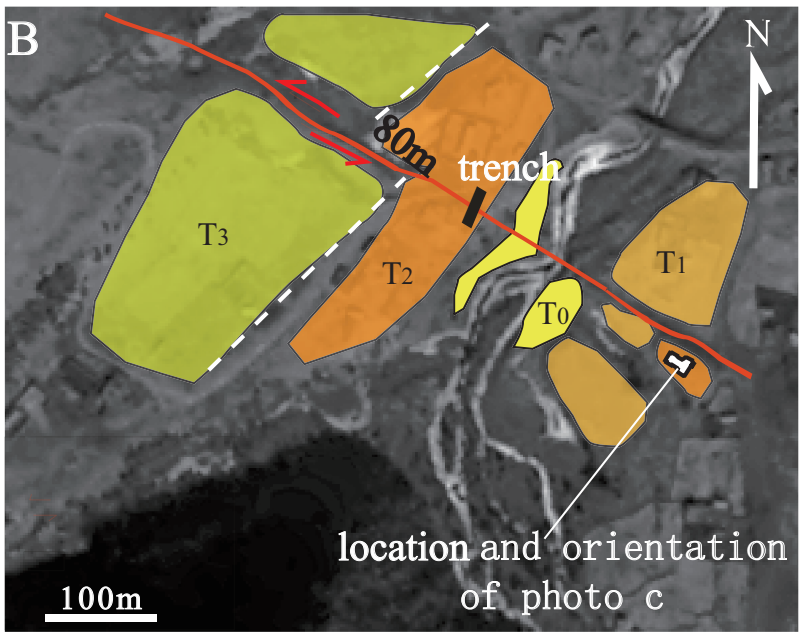
B
N
80m
trench
T3
T2
T1
T0
location and orientation
of photo c
100m

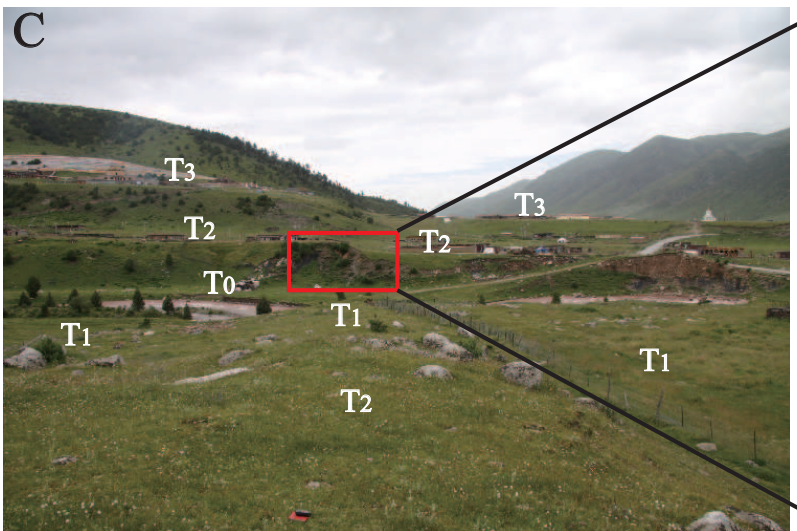
C
T3
T2
T0
T1
T3
T2
T1
T1
T2


D
SW
NE
305°
∠68°

Figure8

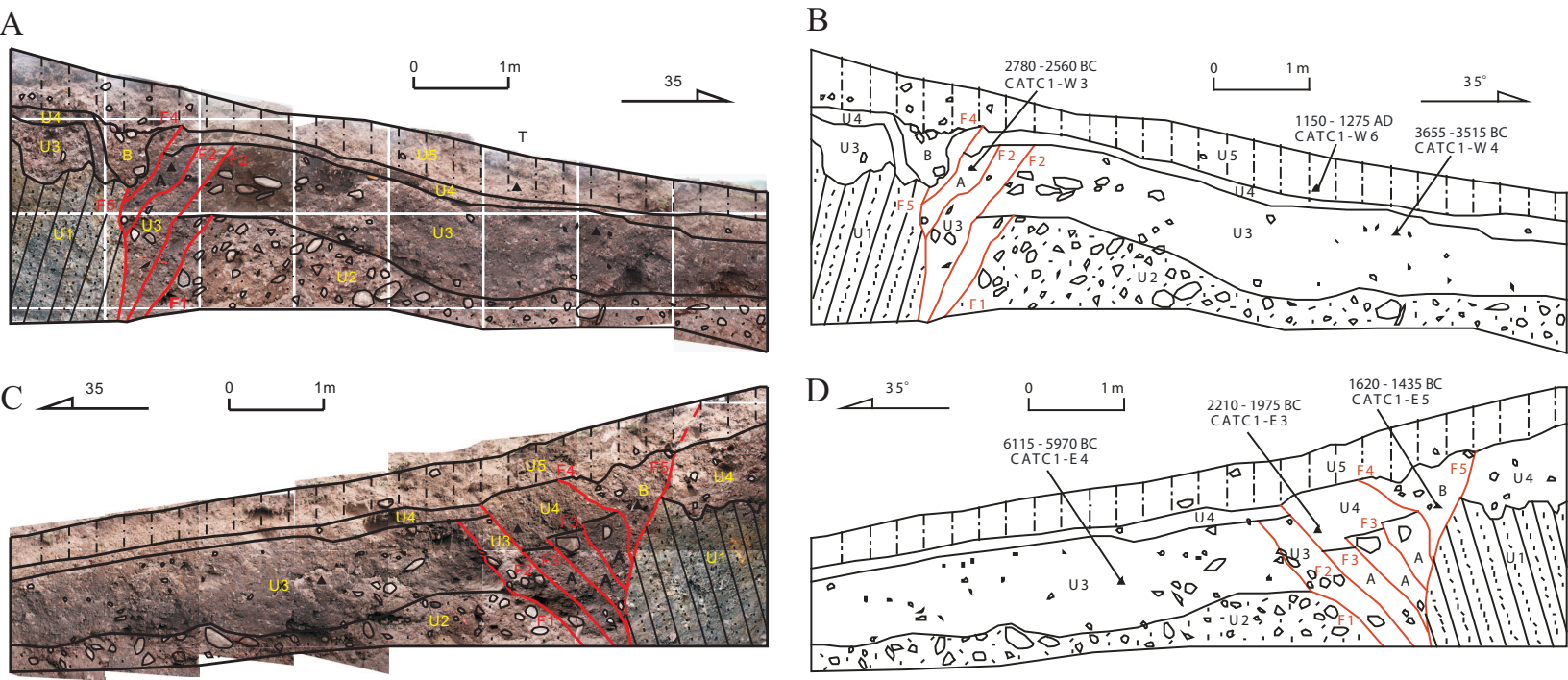
A
0
1m
35
U4
U3
F4
B
F3
F2
U5
T
U4
F5
U1
U3
U3
U2
F1
B
2780 - 2560 BC
CATC1-W3
0
1 m
35°
1150 - 1275 AD
CATC1-W6
3655 - 3515 BC
CATC1-W4
U4
U3
F4
B
F2
F2
U5
U4
F5
U1
U3
U3
U2
F1
C
35
0
1m
U5
F4
F5
B
U4
U4
F4
U4
U3
F3
U1
U3
F2
U2
F1
D
35°
0
1 m
2210 - 1975 BC
CATC1-E3
1620 - 1435 BC
CATC1-E5
6115 - 5970 BC
CATC1-E4
U5
F4
F5
B
U4
U4
U4
F3
U3
F3
A
U1
U3
F2
A
A
U2
F1

Figure9

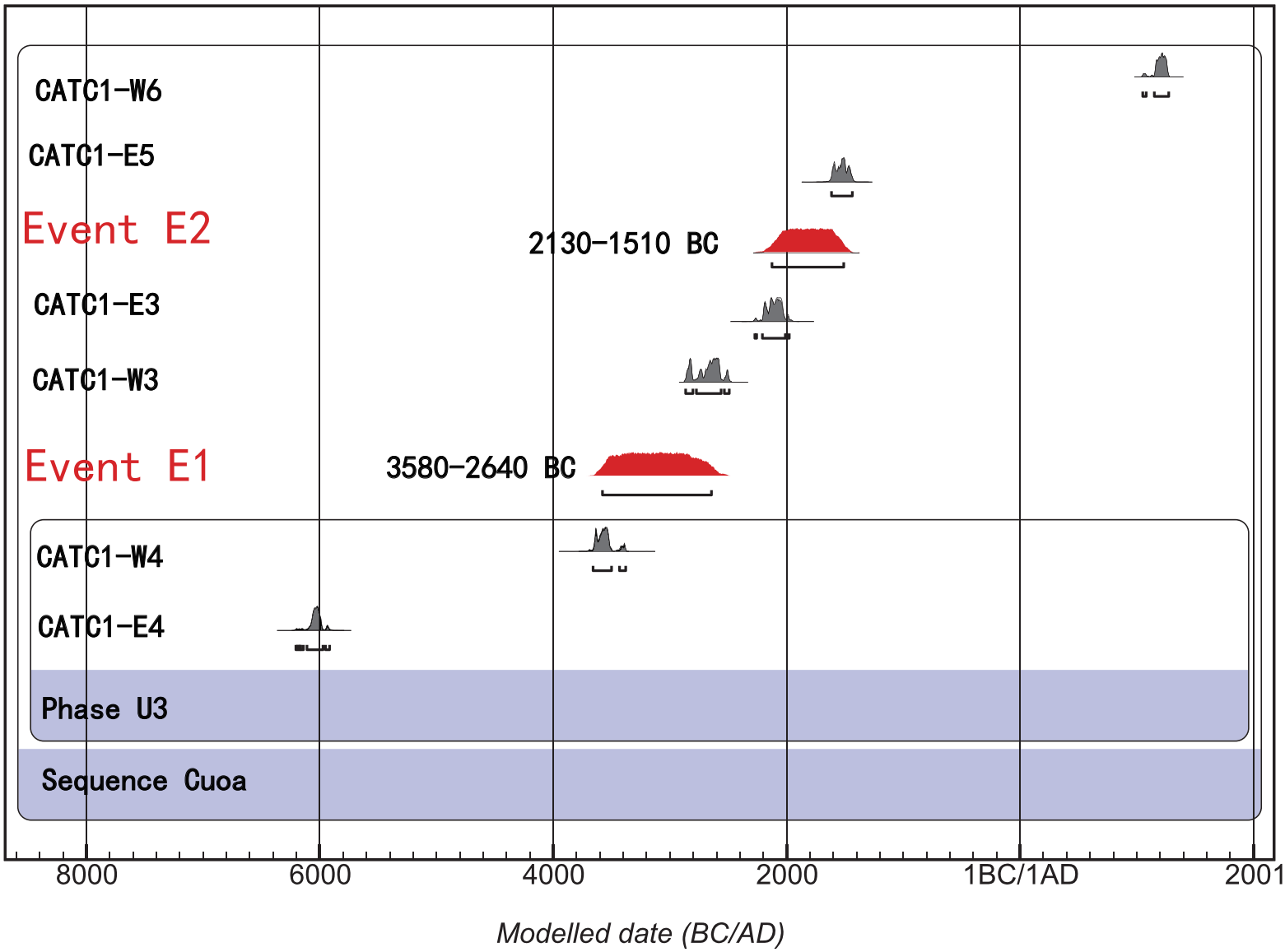
CATC1-W6
CATC1-E5
Event E2
2130-1510 BC
CATC1-E3
CATC1-W3
Event E1
3580-2640 BC
CATC1-W4
CATC1-E4
Phase U3
Sequence Cuoa
8000
6000
4000
2000
1BC/1AD
2001
Modelled date (BC/AD)

Figure10

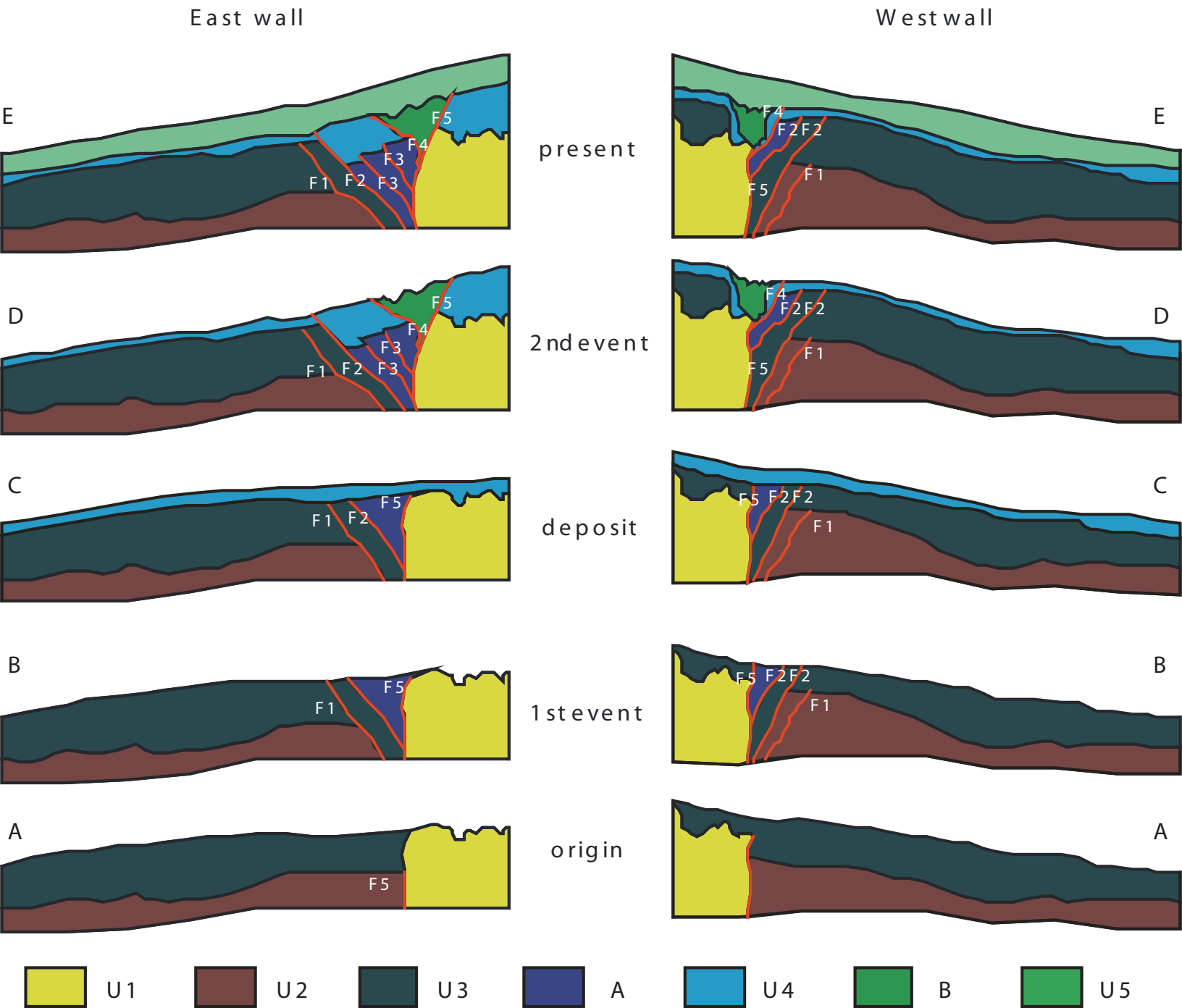
East wall
West wall
E
D
C
B
A
present
2nd event
deposit
1st event
origin
F1
F2
F3
F4
F5
U1
U2
U3
A
U4
B
U5

Figure11

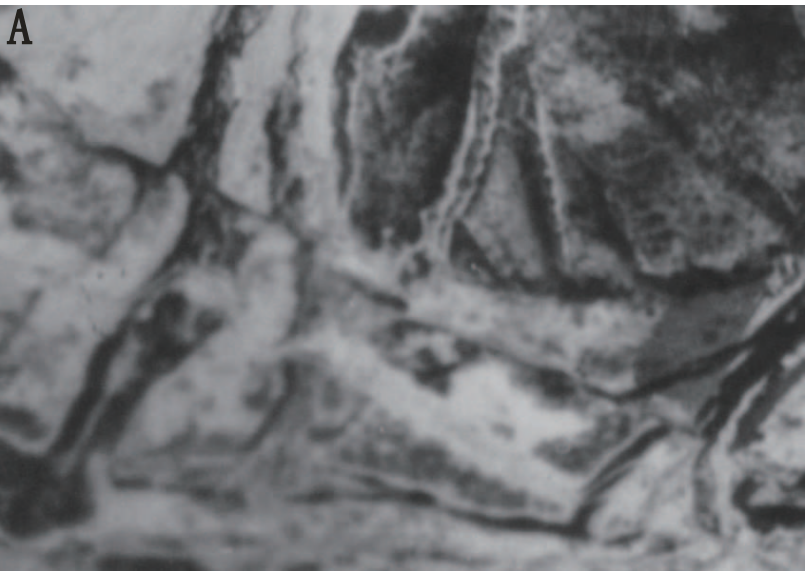

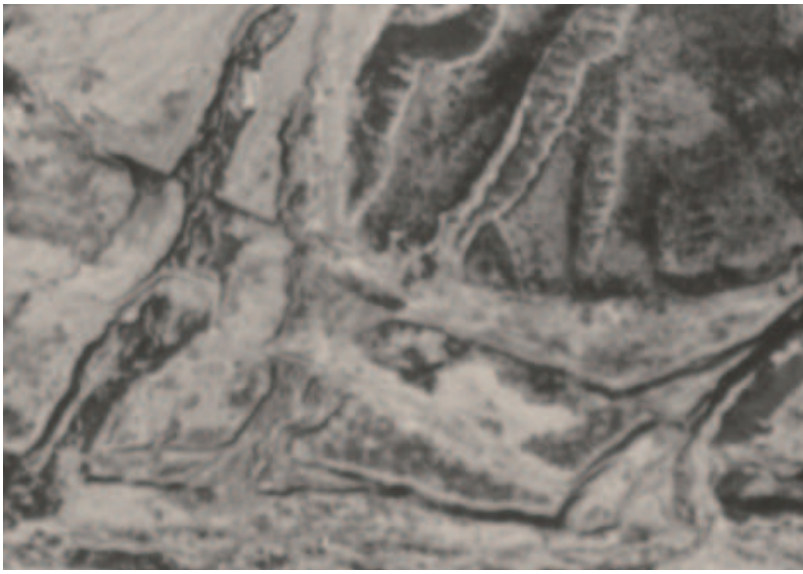

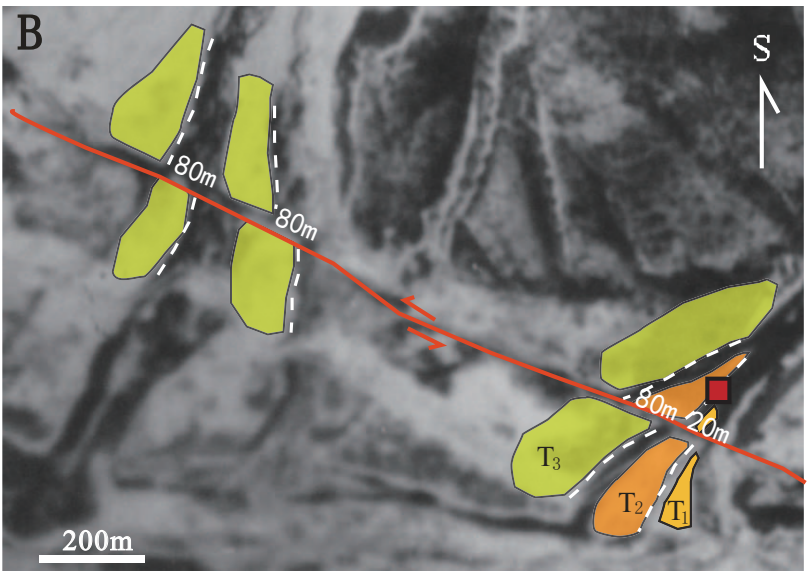

Figure12

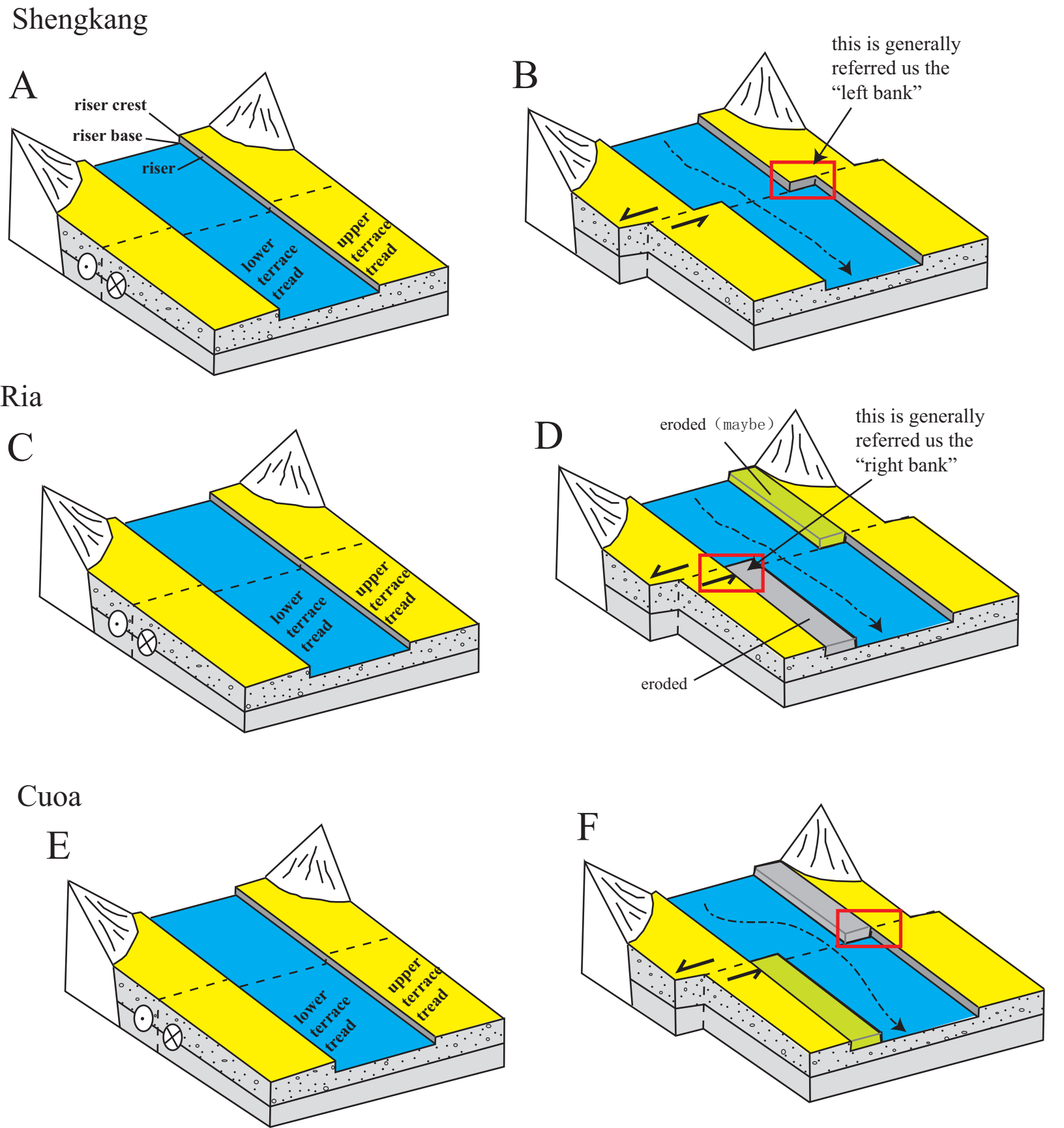
Shengkang
A
riser crest
riser base
riser
lower terrace tread
upper terrace tread
B
this is generally referred us the "left bank"
Ria
C
lower terrace tread
upper terrace tread
D
eroded (maybe)
this is generally referred us the "right bank"
eroded
Cuoa
E
lower terrace tread
upper terrace tread
F

Figure13

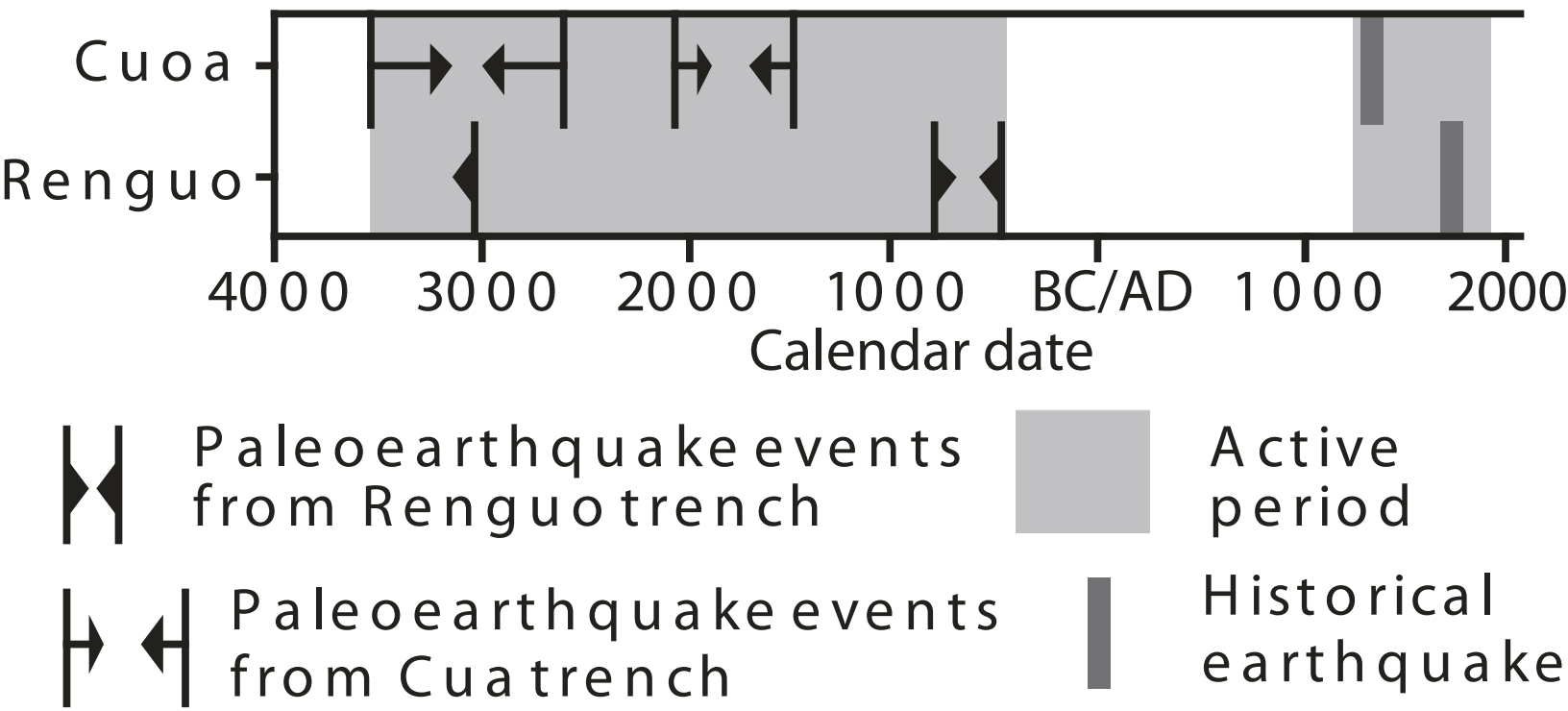
Cuoa
Renguo
4000
3000
2000
1000
BC/AD
1000
2000
Calendar date
Paleoearthquake events from Renguo trench
Active period
Paleoearthquake events from Cua trench
Historical earthquake